

# Reviewer #1

**Comment 1:** The introduction lacks of progresses about research issues.

**Response 1:** We overviewed some more research progresses in Lines 90-93: *Circulation of a strong Siberian High to the north and cold anomalies in the low-level troposphere with strong East Asian Trough is found to be favorable for the clear winter in Beijing and surrounding region (Pei and Yan, 2018).*

And Lines 107-117: *However, compared to the developing phase, which typically features a smooth increase in air pollutant concentrations due to the regional transport, local accumulation and secondary formation, the decay phase of each pollution episode shows a sharp decrease in PM<sub>2.5</sub> concentrations, often in a few hours. Pollutants on hazy days show mass concentration 2-3 times higher than that on clear days (Li et al., 2010). The abrupt decrease in PM<sub>2.5</sub> concentrations is purely meteorological in origin and is controlled by the passage of synoptic systems, especially cold fronts, which terminate a severe air pollution episode in the BTH region by strong winds (Zhu et al., 2016; Jia et al., 2008; Ji et al., 2012; Xin et al., 2012). Many studies took the smooth increase period of PM<sub>2.5</sub> concentrations and abrupt decrease stage following it as a complete air pollution episode, and investigate its development mechanism (Tang et al., 2016b; Zhang et al., 2018b; Sun et al., 2014; Zheng et al., 2015).*

Reference:

Pei, L., and Yan, Z.: Diminishing clear winter skies in Beijing towards a possible future, *Environ. Res. Lett.*, 13, 124029, 2018.

Li, W., Shao, L., and Buseck, P.: Haze types in Beijing and the influence of agricultural biomass burning, *Atmos. Chem. Phys.*, 10, 2010.

Zhu, X., Tang, G., Hu, B., Wang, L., Xin, J., Zhang, J., Liu, Z., Munkel, C., and Wang, Y.: Regional pollution and its formation mechanism over North China Plain: A case study with ceilometer observations and model simulations, *J. Geophys. Res. Atmos.*, 121, 14,574-514,588, 2016.

Jia, Y., Rahn, K. A., He, K., Wen, T., and Wang, Y.: A novel technique for quantifying the regional component of urban aerosol solely from its sawtooth cycles, *J. Geophys. Res. Atmos.*, 113, D21309, 2008.

Ji, D., Wang, Y., Wang, L., Chen, L., Hu, B., Tang, G., Xin, J., Song, T., Wen, T., and Sun, Y.: Analysis of heavy pollution episodes in selected cities of northern China, *Atmos. Environ.*, 50, 338-348, 2012.

Xin, J., Gong, C., Wang, S., and Wang, Y.: Aerosol direct radiative forcing in desert and semi-desert regions of northwestern China, *Atmos. Res.*, 171, 56-65, 2016.

Tang, L., Yu, H., Ding, A., Zhang, Y., Qin, W., Wang, Z., Chen, W., Hua, Y., and Yang, X.: Regional contribution to PM<sub>1</sub> pollution during winter haze in Yangtze River Delta, China, *Sci. Total Environ.*, 541, 161-166, 2016b.

Zhang, X., Zhong, J., Wang, J., Wang, Y., and Liu, Y.: The interdecadal worsening of weather conditions affecting aerosol pollution in the Beijing area in relation to climate warming, *Atmos. Chem. Phys.*, 18, 5991-5999, 2018b.

Sun, Y., Jiang, Q., Wang, Z., Fu, P., Li, J., Yang, T., and Yin, Y.: Investigation of the sources and evolution processes of severe haze pollution in Beijing in January 2013, *J. Geophys. Res. Atmos.*, 119, 4380-4398, 2014.

Zheng, G., Duan, F., Su, H., Ma, Y., Cheng, Y., Zheng, B., Zhang, Q., Huang, T., Kimoto, T., and Chang, D.: Exploring the severe winter haze in Beijing: the impact of synoptic weather, regional transport and heterogeneous reactions, *Atmos. Chem. Phys.*, 15, 2969, 2015.

**Comment 2:** The colors in Figure 3 make the readers confused, need to be modified.

**Response 2:** The probability density function of day-to-day difference of PM<sub>2.5</sub> in Figure 3 has been modified in the revised version.

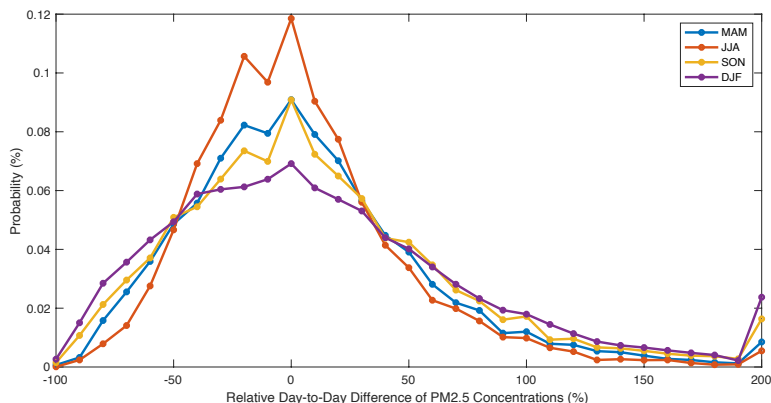


Figure 3. Probability distribution of the relative day-to-day difference of PM<sub>2.5</sub> concentrations. The relative difference is based on the PM<sub>2.5</sub> concentration on the previous day. The distributions in spring and autumn are combined in the upper panel, and cases in winter and summer are shown at the bottom.

**Comment 3:** Line 149, “which is known as a sawtooth cycle”, the adjustment interval of synoptic circulations is related to the period of Rossby waves, which is about 1 week.

**Response 3:** Yes, Rossby wave is the dominating wave system in the mid-latitude region, which has a cycle of about one week. The average interval durations of two decay processes are ranged in 5.36 to 7.45 days in different seasons, according with the cycle length of Rossby wave. Therefore, we added some description in Lines 370-372 to link the decay phase duration and Rossby wave cycle: *As the main wave system affecting the synoptic circulation in mid-latitude region, the Rossby wave has about one-week cycle length, which dominates the average duration of two adjacent decay*

*phase.*

And in Lines 410-412: *The intervals between two continuous decay processes are 5.53, 7.45, 5.86 and 5.36 days from spring to winter, respectively, which may be controlled by the cycle length of Rossby waves in the mid-latitude region.*

**Comment 4:** Line 175, why not to choose other weather typing approaches, such as Lamb-Jenkinson method. It's has no associations with sample data.

**Response 4:** Thanks for your suggestion. We tried the method of Lamb-Jenkinson method in the revised version. The circulation patterns based on the new classification method are similar to that of the principal component analysis (PCA) method as shown in the Supplementary Information (text in SI and Fig. S2-S3), which confirmed the robust of the classification results of PCA method.

We add some description about the Lamb- Jenkinson method in SI: *ERA5 daily mean sea level pressure in Jan. 2014 to Mar. 2020 are used to classify the synoptic circulation types based on Lamb-Jenkinson method. Circulation types are classified into 26 types including eight directional types (northerly, N; northeasterly, NE; easterly, E; southeasterly, SE; southerly, S; southwesterly, SW; westerly, W; and northwesterly, NW), two vorticity types (cyclonic, C; anticyclonic, A) and sixteen hybrid types (CN, CNE, CE, CSE, CS, CSW, CNW, AN, ANE, AE, ASE, AS, ASW, AW and ANW). Figure S2 shows the seasonal frequency of the 26 CTs during Jan. 2014 to Mar. 2020. The frequencies of the two vorticity and eight directional types were much higher than those of other sixteen hybrid CTs. The top four highest frequency for the specific season are highlighted in Fig. S2. Fig. S3 shows the distribution of atmospheric circulation at 925 hPa of the top four highest frequency CTs. Circulation characteristics in Figure S1 has the similar pattern with those in Figure S3, which indicates the robust of the two circulation classification methods.*

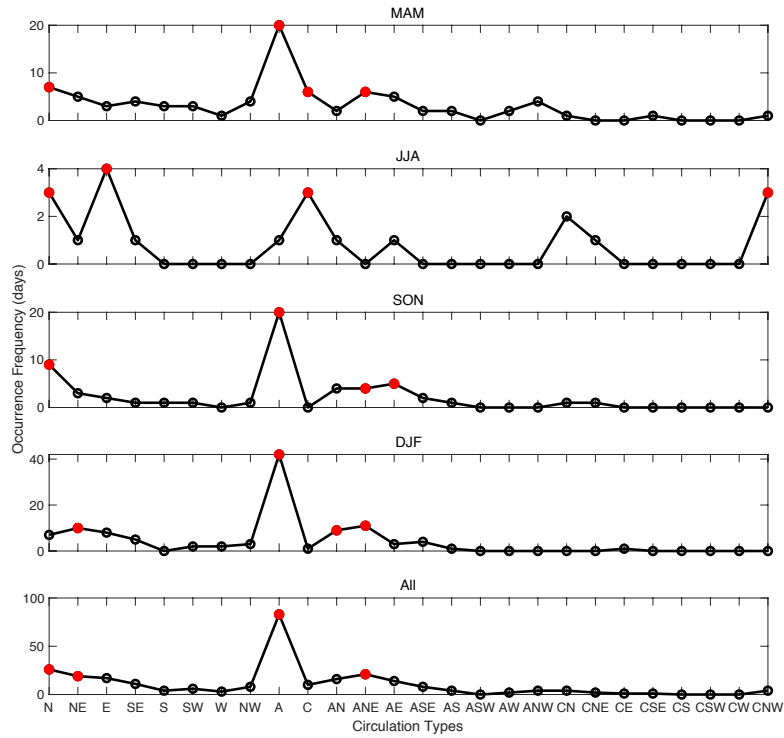


Figure S2. Occurrence frequency of 26 kinds of circulation types based on Lamb-Jenkinson circulation classification method during Jan. 2014 to Mar. 2020. Red dots indicate the top four highest frequency.

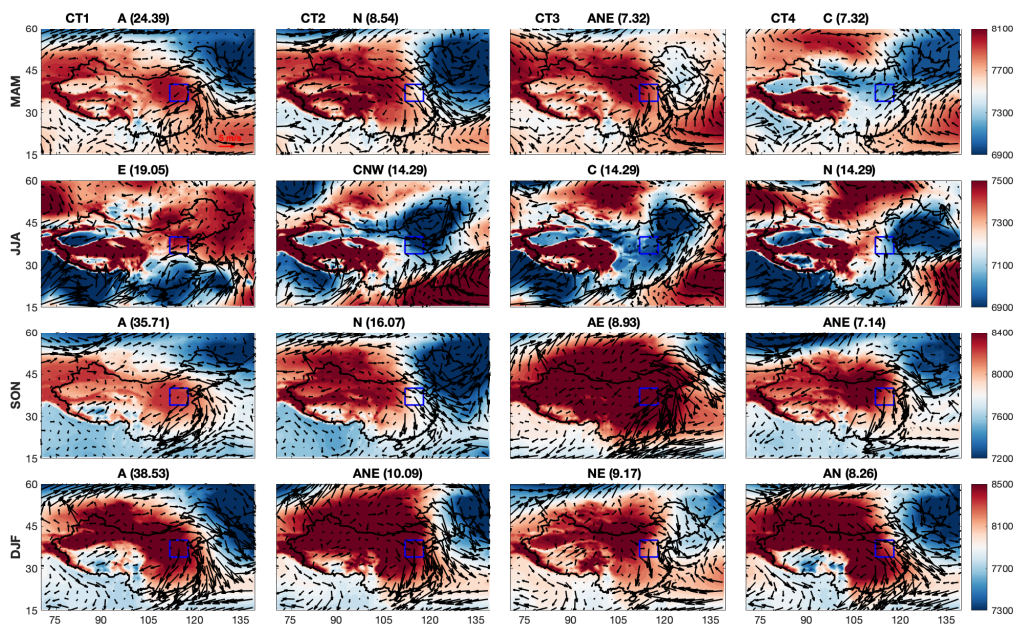


Figure S3. Distribution of the geopotential height (shade, units:  $m^2/s^2$ ) and wind fields at 925 hPa for the top four highest frequency CTs based on Lamb-Jenkinson classification methods. The title of

each subplot indicates the specific CTs and the corresponding frequency (%) in each season.

We also add some description in Lines 193-202 of the main text as: *The Lamb-Jenkinson-Collison type classification (JCT) is also a widely adopted method to identify synoptic circulation pattern by describing the location of cyclonic/anticyclonic centers and the direction of the geostrophic flow (Li et al., 2020; Fan et al., 2015; Jiang et al., 2020; Chen, 2000; Jenkinson and Collison, 1977). In order to verify the robust of circulation classification results of PCA method, JCT method is also involved based on daily mean gridded sea level pressure at 16 points centered by 37° N and 117° E as shown in SI. According to Fig. S1 and Fig. S3, it shows almost the similar circulation pattern of PCA and JCT method, indicating the consistence of two classification methods. Because JCT method is specialized on classifying daily mean sea level pressure patterns, which will ignore the thresholds of some other meteorological variables to some extent. Therefore, we only focus on the results of PCA hereafter.*

Reference:

Li, M., Wang, L., Liu, J., Gao, W., Song, T., Sun, Y., Li, L., Li, X., Wang, Y., and Liu, L.: Exploring the regional pollution characteristics and meteorological formation mechanism of PM<sub>2.5</sub> in North China during 2013–2017, *Environ. Int.*, 134, 105283, 2020.

Fan, L., Yan, Z., Chen, D., and Fu, C.: Comparison between two statistical downscaling methods for summer daily rainfall in Chongqing, China, *Int. J. Climatol.*, 35, 3781-3797, 2015.

Jiang, Y., Xin, J., Wang, Y., Tang, G., Zhao, Y., Jia, D., Zhao, D., Wang, M., Dai, L., and Wang, L.: The dynamic-thermal structures of the planetary boundary layer dominated by synoptic circulations and the regular effect on air pollution in Beijing, *Atmos. Chem. Phys. Discuss.*, 1-21, 2020.

Chen, D.: A monthly circulation climatology for Sweden and its application to a winter temperature case study, *Int. J. Climatol.*, 20, 1067-1076, 2000.

Jenkinson, A., and Collison, F.: An initial climatology of gales over the North Sea, *Synoptic climatology branch memorandum*, 62, 18, 1977.

Philipp, A., Beck, C., Esteban, P., Kreienkamp, F., Krennert, T., Lochbihler, K., Lykoudis, S. P., Pianko-Kluczynska, K., Post, P., and Alvarez10, D. R.: cost733class-1.2 User guide, Augsburg, Germany, 10-21, 2014.

**Comment 5:** Line 270, strong vertical shear? The top of PBL was located between positive and negative wind shear in most cases where the shear is about zero. Have you compared with pollution situations? This may be caused by the air with different properties within or above the PBL.

**Response 5:** Yes, in CT1 condition, the top of the boundary layer located at the transition zone from negative wind shear anomaly to positive anomaly. While, due to westward climbing of the

prevailing easterly wind, low-level air pollutants are taking out of the boundary layer. As long as the air pollutants are brought to the free atmosphere, they will be well blended quickly due to the upper-level strong wind shear.

According to your suggestion, 24 h backward trajectories of Beijing are conducted based on NOAA HYSPLIT Trajectory model using NECP reanalysis dataset. Fig. S6 shows the surface (10 m) and free atmosphere (2000 m above ground level) 24 h backward trajectories of each decay phase day. We can find that the air mass within and above the boundary layer almost come from the same direction in a specific circulation type, which indicates the consistence air mass properties from the surface to the free atmosphere. In addition, most of the backward trajectories come from west and northwest of Beijing, which brings cold and dry air mass and benefits for the decay of pollution episodes. We add the description in Lines 302-303: *According to the distribution of 24 h backward trajectories of Beijing in Fig. S6, the northwesterly cold and dry air mass are taking to the domain, benefiting for the decay of local pollution episodes.*

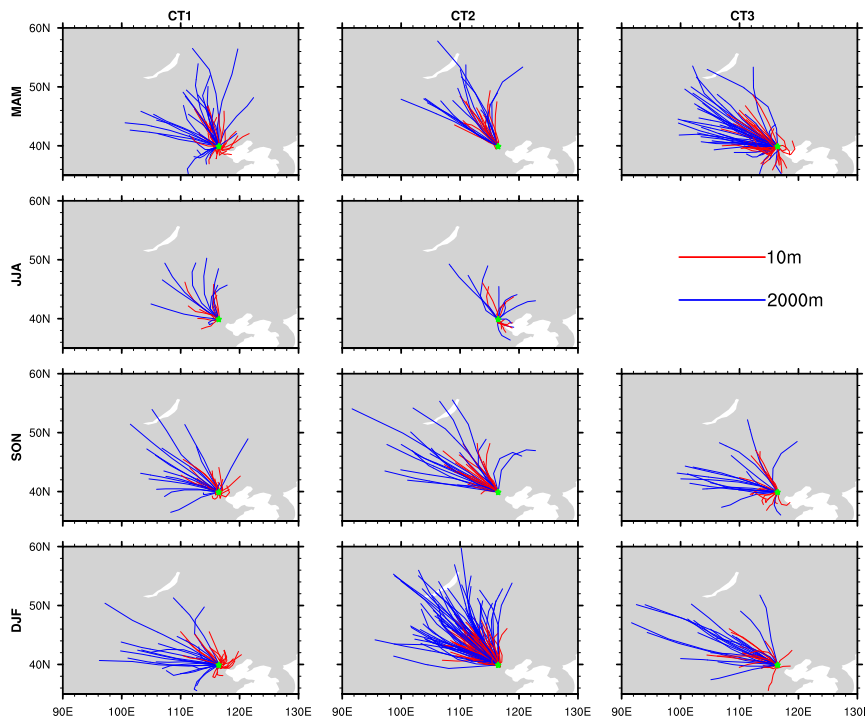


Figure S6. 24 h backward trajectories of Beijing at 10 m and 2000 m (above ground level) on all the decay phase days based on the NOAA HYSPLIT Trajectory model.

**Comment 6:** Line 412, horizontal wind shear, do you mean vertical shear of horizontal winds?

**Response 6:** Yes, it should be vertical shear of horizontal winds. We have revised it in the new version.

**Comment 7:** About the primary conclusions in paper, we have already known that meteorological conditions, such as strong winds and low relative humidity, are favorable for removing pollutants. However, in CT1, pollutants within PBL diffused upward, while flows presented to be sinking motion in CT2 and CT3 in contrast. What is the leading mechanism for removing pollutants in different patterns?

**Response 7:** The prevailing wind direction is easterly wind in CT1, which will climb westward due to the western mountain region and in turn brings the surface air pollutants out of the boundary layer. While, in CT2 and CT3 conditions, the air mass crossing the mountain will motivate a downward motion, which is known as the downwash airflow due to blocking of mountainous terrain. In CT2, it is the strongest positive wind anomaly, positive boundary layer height anomaly and negative relative humidity that leads to the quickly decay of air pollution, which is the commonly believed synoptic circulation breaking off pollution episodes over northern China. The cleaning performance of CT2 is the strongest among the three kinds of circulation types. CT3 also has positive wind speed anomaly and negative relative humidity anomaly, but the magnitudes of anomalies are not as significant as those of CT2. Stronger than normal vertical mixing within the boundary layer may contribute to the decrease in air pollutant concentrations. Although PM<sub>2.5</sub> concentration will decrease by 27~29% after the passage of CT3, the removal efficiency of CT3 is the weakest among the three CTs, which can be attributed to the moderate favorable horizontal diffusion conditions. We clarified the cleaning mechanisms in the Conclusion section in Lines 413-427: *All the CTs are common in positive wind speed anomaly, negative relative humidity anomaly and effective outflow of PM<sub>2.5</sub> from the domain. Although the magnitude and significance of the anomalies are different in the specific CT, all the above variables indicate favorable atmospheric diffusion conditions, which is benefit for the decay of pollution episodes. There are also some prominent features for each CT. In CT1, the most significant horizontal outflow of air pollutants combining with the upward transport of airflow to the free atmosphere are the two extra drivers for the decay processes. The removal efficiency of CT1 is 35-40%, which is moderate among the three CTs. In terms of CT2, it is the most frequent CT in autumn and winter. The circulation with the heaviest wind speed from the northwest, the highest BLH, lowest relative humidity jointly results in the quickly decrease in PM<sub>2.5</sub> concentration in a few hours, which is the commonly accepted circulation feature to terminate the severe pollution episodes. Due to the significantly favorable meteorological conditions, CT2 has the strongest cleaning abilities of 41-45% in different seasons. For CT3, the synergy effects of enhanced vertical mixing within the boundary layer and moderate beneficial background of wind speed, relative humidity and horizontal divergence of PM<sub>2.5</sub> are the main cleaning mechanism of CT3 condition.*

And add some discussions in Lines 440-444: *PM<sub>2.5</sub> concentrations sharply decrease after the*

*passage of CT2, but it shows a relatively weak drop in air pollutant concentrations when CT3 occurs, which can be attributed to its moderate strength of anomalies circulation pattern. Therefore, the scavenging effects of each CT should also be taken into account when predicting the air quality based on synoptic circulation variation.*

**Comment 8:** How much is the contribution of horizontal advection and vertical diffusion respectively for removing pollution in different types and seasons? And mainly through which layer do pollutants diffuse downstream?

**Response 8:** The net PM<sub>2.5</sub> flux of horizontal and vertical direction is an ideal metric to evaluate the outflow or inflow of air pollutants from a domain. High temporal (daily at least) and spatial resolution (grid scale at least) PM<sub>2.5</sub> profile and 3-D wind fields are needed to measure the contribution of vertical diffusion. However, the grid scale daily PM<sub>2.5</sub> profiles are not available currently. Satellite data, e.g., CALIPSO Level 2 aerosol profiles, could provide aerosol profiles with 5 km horizontal resolution, but its limit temporal resolution (with a repeat cycle of 16-day) does not meet the requirement. We added the discussion about this in Lines 435-440: *Due to the limitation of dataset about PM<sub>2.5</sub> vertical distribution, only the horizontal divergence of PM<sub>2.5</sub> flux is used in this study. Although it shows positive divergence for all the CTs, indicating the remarkable contribution of the net outflow of air pollutants at the surface to the quickly decrease in PM<sub>2.5</sub> concentrations, the effects of horizontal PM<sub>2.5</sub> flux above the surface or the vertical diffusion cannot be neglected, which may have great contribution in a specific event, and need to be further studies.*

In addition, the horizontal divergence of PM<sub>2.5</sub> flux is further refined to four directions in Fig. S4, which shows more detailed information of flux from each side. For CT1, the horizontal PM<sub>2.5</sub> flux divergence is the most positive, with significant outflow of air pollutants from in the southern edge of the domain. The magnitude of inflow from eastern side is at the same level as the outflow from western edge, leading to the insignificant zonal divergence. For CT2, significant positive divergence in the eastern and southern edges contribute to the net outflow of air pollutants. In terms of CT3, the zonal divergence of the PM<sub>2.5</sub> flux dominates the net positive divergence of the whole region, rather than the meridional component as the other two circulation patterns.



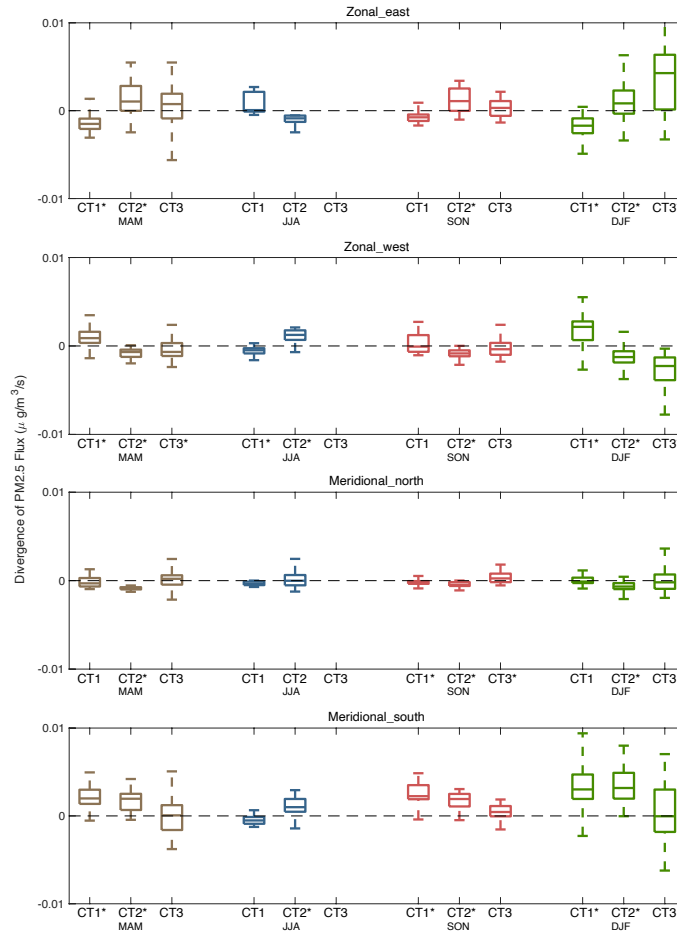


Figure S4. Boxplot of the divergence of PM2.5 flux from the four sides of the region of 34-40° N and 112-118° E. Positive divergence indicates outflow of PM2.5 from the specific direction; negative divergence indicates inflow of PM2.5 from the domain. \* in the x axis marks the divergence in a specific CT is significantly different with zero based on two-tail student-t test at a significant level of 0.01.

**Comment 9:** The whole paper needs to be more standard and concise. Some conclusions are moved to the discussion section. The removing mechanisms in different synoptic patterns need to be more clarified.

**Response 9:** Thanks for your suggestion. We reorganized the abstract and conclusion sections to clarify the removing mechanism of each circulation type.

Abstract section in Lines 35-39: *CT2 is the most frequent CT in autumn and winter, with the highest wind speed from the northwest, the highest boundary layer height (BLH), and lowest relative humidity among the three CTs, all of which are favorable for the reduction of PM2.5 concentrations. In CT3, strong vertical wind shear within the boundary layer enhances the mixing of surface air*

*pollutants, which is the extra cleaning mechanism besides dry and clean air mass inflow.*

*Conclusion section in Lines 413-444: All the CTs are common in positive wind speed anomaly, negative relative humidity anomaly and effective outflow of PM<sub>2.5</sub> from the domain. Although the magnitude and significance of the anomalies are different in the specific CT, all the above variables indicate favorable atmospheric diffusion conditions, which is benefit for the decay of pollution episodes. There are also some prominent features for each CT. In CT1, the most significant horizontal outflow of air pollutants combining with the upward transport of airflow to the free atmosphere are the two extra drivers for the decay processes. The removal efficiency of CT1 is 35-40%, which is moderate among the three CTs. In terms of CT2, it is the most frequent CT in autumn and winter. The circulation with the heaviest wind speed from the northwest, the highest BLH, lowest relative humidity jointly results in the quickly decrease in PM<sub>2.5</sub> concentration in a few hours, which is the commonly accepted circulation feature to terminate the severe pollution episodes. Due to the significantly favorable meteorological conditions, CT2 has the strongest cleaning abilities of 41-45% in different seasons. For CT3, the synergy effects of enhanced vertical mixing within the boundary layer and moderate beneficial background of wind speed, relative humidity and horizontal divergence of PM<sub>2.5</sub> are the main cleaning mechanism of CT3 condition. After the passage of CT3, 26~29% of local air pollutants are typically removed. The two dry-day circulation patterns in summer are similar to the synoptic patterns of CT1 and CT3 in the other three seasons. A dry air mass with a positive BLH anomaly and the effective horizontal outflow of air pollutants are the main reasons for the abrupt decay phases in summer. The average PM<sub>2.5</sub> concentrations on decay process days show a significant decreasing trend from 2014 to 2020, which indicates the success of emission mitigation efforts. Emission reductions have led to a 4.3~5.7  $\mu\text{g}/(\text{m}^3\cdot\text{yr})$  decrease in PM<sub>2.5</sub> concentrations in the 28 pollution channel cities.*

*Due to the limitation of dataset about PM<sub>2.5</sub> vertical distribution, only the horizontal divergence of PM<sub>2.5</sub> flux is used in this study. Although it shows positive divergence for all of the CTs, indicating the remarkable contribution of the net outflow of air pollutants at the surface to the quickly decrease in PM<sub>2.5</sub> concentrations, the effects of horizontal PM<sub>2.5</sub> flux above the surface or the vertical diffusion cannot be neglected, which may have great contribution in a specific event, and need to be further studies. PM<sub>2.5</sub> concentrations sharply decrease after the passage of CT2, but it shows a relatively weak drop in air pollutant concentrations when CT3 occurs, which can be attributed to its moderate strength of anomalies circulation pattern. Therefore, the scavenging effects of each CT should also be taken into account when predicting the air quality based on synoptic circulation variation.*

## Reviewer #2

**Comment 1:** Lines 28–30, “the same three circulation types (CTs)...” does not make sense, cause only two CTs were mentioned before.

**Response 1:** We revised the sentence as in Lines 29-30 “*Two dominant circulation patterns are identified in summer. All the other three seasons have three circulation types (CTs), respectively. The three CTs in spring show the same patterns with those in autumn and winter*”.

**Comment 2:** In Abstract, it’s better to define CT1, CT2, and CT3 first and then discuss their impacts on PM2.5 decay processes.

**Response 2:** Thanks for your suggestion. We reorganized the removing mechanisms of each CT in the abstract section in Lines 30-41: *The circulation patterns beneficial to the decay processes all exhibit a higher-than-normal surface wind speed, a negative relative humidity anomaly and net outflow of PM2.5 from the domain. In addition, CT1 in spring, autumn and winter is controlled by northeasterly wind and features the most significant horizontal net-outflow of air pollutants and effective upward spread of air pollutants to the free atmosphere. CT2 is the most frequent CT in autumn and winter; with the highest wind speed from the northwest, the highest boundary layer height (BLH), and lowest relative humidity among the three CTs, all of which are favorable for the reduction of PM2.5 concentrations. In CT3, strong vertical wind shear within the boundary layer enhances the mixing of surface air pollutants, which is the extra cleaning mechanism besides dry and clean air mass inflow. PM2.5 concentrations show significant decreases of more than 37%, 41% and 27% after the passage of CT1, CT2 and CT3, respectively.*

**Comment 3:** Line 130, it should be “in a specific region,”

**Response 3:** Revised as suggested.

**Comment 4:** Line 208, delete “of”.

**Response 4:** Revised as suggested.

**Comment 5:** How a dry day is defined? Is it defined for each grid cell or for the entire study domain? Is it defined as a day with zero precipitation or with precipitation less than a threshold? What precipitation data were used?

**Response 5:** ERA5 hourly total precipitation dataset with a resolution of  $0.5^{\circ} \times 0.5^{\circ}$  is used in this study. The domain region covering the 28 cities is  $36^{\circ}$ - $42^{\circ}$  N and  $113^{\circ}$ - $117.5^{\circ}$  E. If the daily mean accumulated precipitation amount is larger than 1 mm for all the grid cells in the domain, the day is defined as a rainy day with effective wet deposition. We added the defined of dry days in the text in Line 135-136: *Daily accumulated precipitation amount is the total amount of 24-hour values.*

And in Lines 224-228: *If the daily mean accumulated precipitation amount is more than 1 mm for all the grid cells in the region of  $36^{\circ}$ - $42^{\circ}$  N and  $113^{\circ}$ - $117.5^{\circ}$  E (covering the 28 cities), the specific day is defined as a rainy day with effective wet deposition. 97 of the 365 decay phases are defined as rainy days, in which case the abrupt decrease in ambient PM<sub>2.5</sub> concentrations are assumed to be related to wet deposition.*

**Comment 6:** Line 211, should be “a specific year”.

**Response 6:** Revised as suggested.

**Comment 7:** Figure 8, the four variables in each circulation type and each season should be tested to see if they are statistically different from the corresponding seasonal means. The variables that past the significant test should be highlighted in the figure and described in the text.

**Response 7:** The mean values for all the four meteorological variables in each circulation in original Fig. 8 (Fig. 7 in the new version) are significantly different with their seasonal mean based on two-tail student-t test at a significant level of 0.01. The result of significant test was added in the figure caption of Fig. 7. In addition, the student-t test is also conducted to the divergence distribution of PM<sub>2.5</sub> flux in Fig. 8 and Fig. S2. \* is used to highlight the circulation with significant positive or negative divergence.

**Comment 8:** Figure 13, the method to estimate the linear trend should be mentioned and corresponding p values or uncertainties of these trends should be included.

**Response 8:** Least squares regression is used to estimate the linear trend of the monthly median PM<sub>2.5</sub> variations. R-square and p-value for each of the regression model was involved in Fig. 12 (original Fig. 13), which shows significant decrease in PM<sub>2.5</sub> concentrations in spring, summer, autumn during 2014 to 2019. The corresponding description was added in the figure caption.

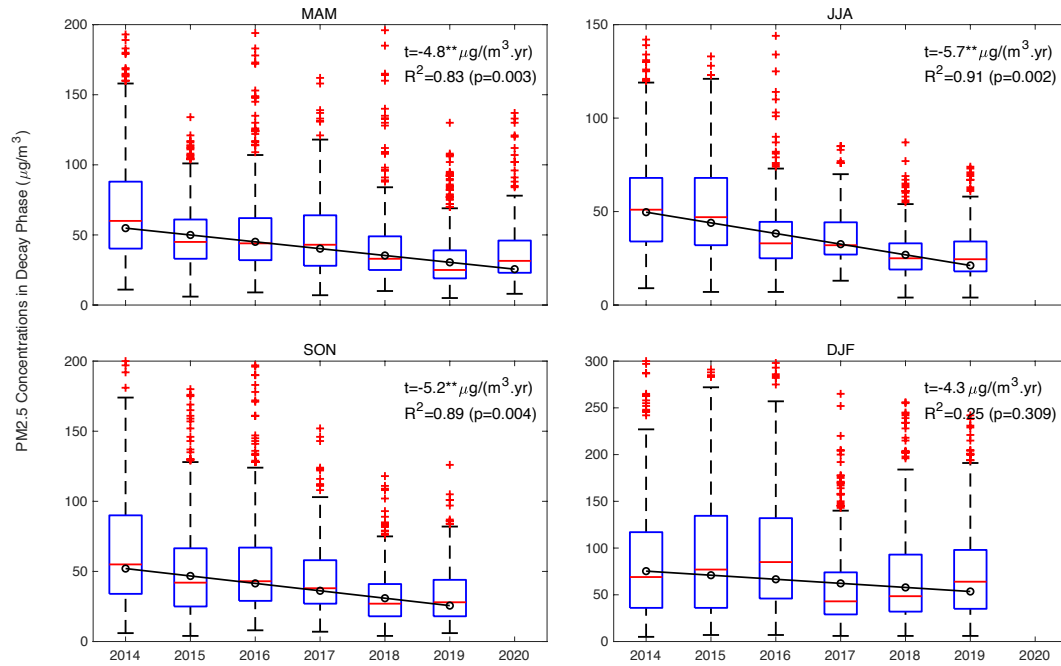


Figure 12. Variations in the average PM<sub>2.5</sub> concentration on all the decay phase days from 2014 to 2020. The black hollow circles indicate the mean PM<sub>2.5</sub> concentration in each year. The black line is the fitting line based on the monthly median value. The number in the subplot is the linear trend (t), R-square and p-value of least squares regression model. \*\* after linear trend indicates the linear regression model is significant with a p-value<0.01.

**Comment 9:** Figure 5 gives similar information to Figure 6, and may be moved to supplementary document.

**Response 9:** Fig. 5 has been moved to the supplementary information in the revised version. Moreover, the distribution of geopotential height anomalies at 500 hPa was also involved in the supplementary.

**Comment 10:** Figure 1 can be modified to add topography information as shadings, since topography is also an important factor that influences the dilution of the pollutants.

**Response 10:** Thanks for your suggestion. The terrain distribution based on the Global Digital Elevation Model was added in Fig. 1.

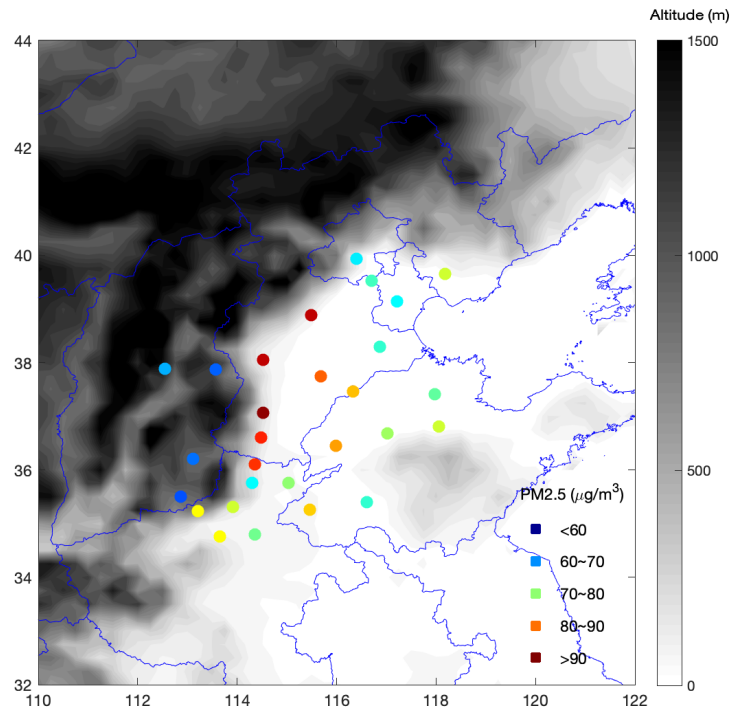


Figure 1. Distribution of annual mean PM2.5 concentrations in the 28 cities by altitude. The PM2.5 concentration is the annual mean value from 2014 to 2019 (units:  $\mu\text{g}/\text{m}^3$ ). The elevation over the domain was obtained from Global Digital Elevation Model with a resolution of  $0.5^\circ \times 0.5^\circ$ .

**Comment 11:** Figure 2 can be improved by showing the mean across the 28 cities with shadings indicating the range of PM2.5. The current figure is a little noisy to observe the sharp decay process.

**Response 11:** Thanks for your suggestion. We revised Fig. 2 with PM2.5 concentrations at the 28 cities displaying by their range.

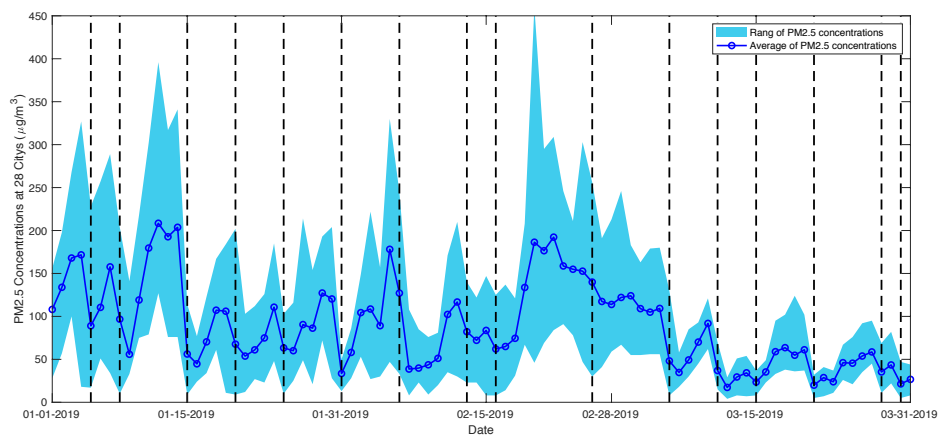


Figure 2. Time series of daily mean PM2.5 concentrations in the 28 pollution channel cities from

January to March 2019 (units:  $\mu\text{g}/\text{m}^3$ ).

**Comment 12:** It is interesting to show the corresponding time series (i.e., principle components) of each circulation type in Figure 5 and to check if there are any temporal trends. If there are trends, then the decreasing trends in Figure 13 can be partially attributed to circulation changes besides emission changes.

**Response 12:** The time series of each circulation type (CT) frequency can be obtained by year or season as shown in Fig. R1, which has no obvious correspondence with PM<sub>2.5</sub> variations in Fig. 12 (original Fig. 13). The interannual variation of seasonal mean PM<sub>2.5</sub> concentrations may be closely related to the change of seasonal occurrence frequency of a specific CT or their accumulated frequency. In addition, the average interval between two decay progresses may also affect the final seasonal mean PM<sub>2.5</sub> concentrations. We have analyzed the combined effects of CT frequency and their interval on the interannual variation of PM<sub>2.5</sub> concentrations in our previous work ([doi.org/10.5194/acp-20-7667-2020](https://doi.org/10.5194/acp-20-7667-2020)). However, Fig. 12 shows the interannual variation of PM<sub>2.5</sub> concentrations only on the decay phase days instead of the seasonal mean value. If we suppose it has the same scavenging ability for all the decay phase CTs, i.e., the effects of meteorological conditions to air quality remain the same; PM<sub>2.5</sub> after the decay phase would indicate the background air pollutant concentration of ambient environment. Therefore, the long-term variation of the background concentrations can represent the change of emission to a certain extent.

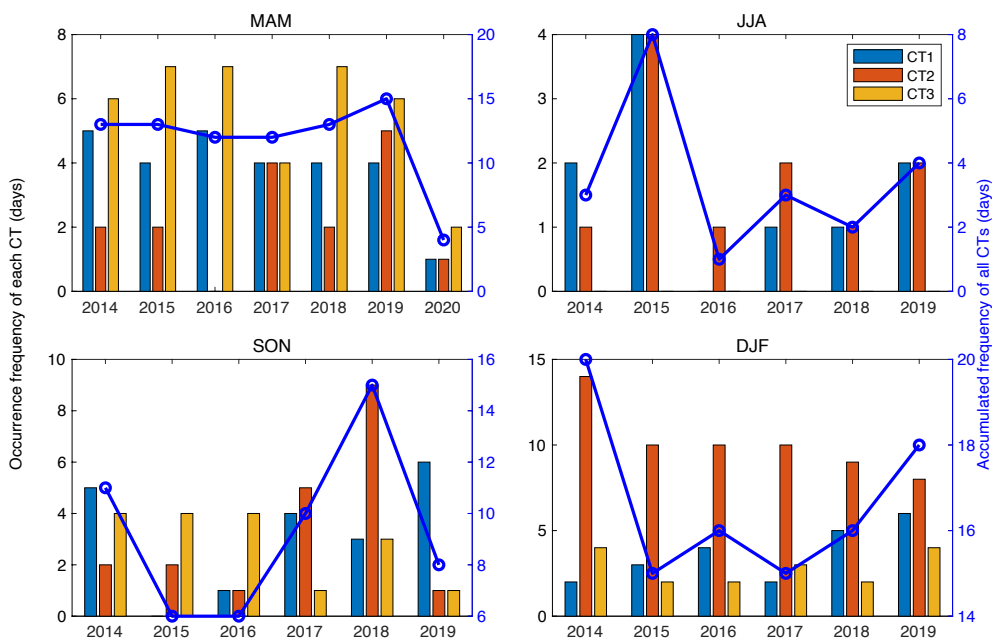


Figure R1. Interannual variation of seasonal occurrence frequency for each CT (left axis) and accumulated frequency for all the three CTs (right axis).

1 **Dominant synoptic patterns associated with the decay process of**  
2 **PM2.5 pollution episodes around Beijing**

3 Xiaoyan Wang<sup>1,2,3\*</sup>, Renhe Zhang<sup>1,2</sup>, Yanke Tan<sup>1,2</sup>, Wei Yu<sup>1,4</sup>

4 <sup>1</sup>Department of Atmospheric and Oceanic Sciences & Institute of Atmospheric Sciences, Fudan  
5 University, Shanghai, China

6 <sup>2</sup>Big Data Institute for Carbon Emission and Environmental Pollution, Fudan University, Shanghai,  
7 China

8 <sup>3</sup>Shanghai Institute of Pollution Control and Ecological Security, Shanghai, China

9 <sup>4</sup>Shanghai Ecological Forecasting and Remote Sensing Center, Shanghai, China

10

11

12 Correspondence to: Xiaoyan Wang (wangxyfd@fudan.edu.cn)

13

14



## 15 Abstract

16 The variation in the concentrations of ambient PM<sub>2.5</sub> (particles with an aerodynamic diameter less  
17 than 2.5 μm) generally forms a continuous sawtooth cycle with a recurring smooth increase followed  
18 by a sharp decrease. The abrupt decay of pollution episode is mostly meteorological in origin, and  
19 is controlled by the passage of synoptic systems. One affordable and effective measure for the  
20 quickly reducing PM<sub>2.5</sub> concentrations in northern China is to wait for strong wind to arrive.  
21 However, it is still unclear how strong the wind needs to be and exactly what kind of synoptic system  
22 most effectively results in the rapid decay of air pollution episodes. PM<sub>2.5</sub> variations over the 28  
23 pollution channel cities of Beijing are investigated to determine the mechanisms by which synoptic  
24 patterns affect the decay processes of pollution episodes. This work shows more obvious day-to-  
25 day variations in PM<sub>2.5</sub> concentration in winter than in summer, which implies that wintertime  
26 PM<sub>2.5</sub> variations are more sensitive to meteorological factors. There were 365 decay processes from  
27 January 2014 to March 2020, and 97 of them were related to the effective wet deposition. 26%~43%  
28 of PM<sub>2.5</sub> pollutant is removed by the wet deposition in different seasons. Two dominant circulation  
29 patterns are identified in summer. ~~All the other three seasons have three circulation types (CTs),~~  
30 ~~respectively. The three CTs in spring show the same patterns with those in autumn and winter.~~ The  
31 circulation patterns beneficial to the decay processes all exhibit a ~~higher-than-normal~~ surface wind  
32 speed, a negative relative humidity anomaly and ~~net outflow of PM<sub>2.5</sub> from the domain~~. In addition,  
33 CT1 in spring, autumn and winter is controlled by northeasterly wind and features the most  
34 significant horizontal net-outflow of air pollutants and effective upward spread of air pollutants to  
35 the free atmosphere. ~~CT2 is the most frequent CT in autumn and winter, with the highest wind speed~~  
36 ~~from the northwest, the highest boundary layer height (BLH), and lowest relative humidity among~~  
37 ~~the three CTs~~, all of which are favorable for the reduction of PM<sub>2.5</sub> concentrations. In CT3, strong  
38 ~~vertical wind shear within the boundary layer enhances the mixing of surface air pollutants, which~~  
39 ~~is the extra cleaning mechanism besides dry and clean air mass inflow.~~ PM<sub>2.5</sub> concentrations show  
40 significant decreases of more than 37%, 41% and 27% after the passage of CT1, CT2 and CT3,  
41 respectively. A dry air ~~flow~~, with a positive BLH anomaly and the effective horizontal outflow of air  
42 pollutants are the main reasons for the abrupt decay phase in summer. PM<sub>2.5</sub> concentrations after  
43 the decay process show a significant decreasing trend from 2014 to 2020, reflecting successful  
44 emission mitigation. Emission reductions have led to a 4.3~5.7 μg/(m<sup>3</sup>.yr) decrease in PM<sub>2.5</sub>  
45 concentrations in the 28 pollution channel cities of Beijing.

46

删除的内容: , and the same three

删除的内容:

删除的内容: are identified in the other three seasons based on the dry-day cases.

删除的内容: higher than normal

删除的内容: positive divergence in the PM<sub>2.5</sub> horizontal flux

删除的内容: , which promotes the abrupt reduction of local PM<sub>2.5</sub> concentrations.

删除的内容: CT2 is the most frequent synoptic pattern leading to decay processes in autumn and winter, and the domain region is located to the east of an anticyclone system. CT2 features a strong northwesterly wind of 2.98~3.88 m/s, the lowest relative humidity and the highest boundary layer height (BLH) among the three CTs

删除的内容: a prevailing westerly wind anomaly occurs in the domain, with remarkable zonal divergence in the PM<sub>2.5</sub> flux and

删除的内容: horizontal

删除的内容: in the near-surface under the boundary layer.

删除的内容: mass

## 68 1. Introduction

69 PM2.5 pollution (particles with an aerodynamic diameter less than 2.5  $\mu\text{m}$ ) has become a severe  
70 threat and challenge in China, especially in the Beijing-Tianjin-Hebei (BTH) region, and has  
71 attracted significant concern regarding how to improve regional air quality (Che et al., 2019; Wang  
72 et al., 2019a; Xia et al., 2016; Zhang et al., 2018a; Mu and Zhang, 2014; Cai et al., 2017; Wang et al.,  
73 2015). To avoid the severe negative impacts of air pollution on public health, the Chinese  
74 government has issued a number of policies to improve the atmospheric environment (Ding et al.,  
75 2019; Chen and Wang, 2015; Zhao et al., 2019; Li et al., 2018b). For example, in September 2013,  
76 the State Council issued the Air Pollution Prevention and Control Action Plan (referred to as Clean  
77 Air Action), which required the BTH region to reduce its PM2.5 concentrations by 25% within 5  
78 years (China's State Council, 2013). With the deep research on the prevention and control of air  
79 pollution, the regional effects of air pollution from cities in the pollution transmission channel in  
80 the BTH region have been highlighted (China Daily, 2017). Therefore, the Work Plan for Air  
81 Pollution Prevention and Control in Beijing, Tianjin, and Hebei and Surrounding Areas was released  
82 in March 2017 (China's State Council, 2018). Much stricter, more comprehensive, and more  
83 detailed prevention and control measurements were taken in the "2+26" cities, including Beijing,  
84 Tianjin, and 26 other cities in the provinces of Hebei, Shandong, Henan and Shanxi. Due to the  
85 persistent efforts towards emission mitigation, the air quality has shown significant improvement in  
86 these 28 pollution channel cities in recent years (Zhang et al., 2019a; Zhang et al., 2019b; Zheng  
87 et al., 2018; Wang et al., 2019d; Gui et al., 2020).

88 Meteorological conditions are considered as one of the important factors for the variation in ambient  
89 PM2.5 pollution, especially for the temporal evolution of each air pollution episode (Zhang et al.,  
90 2014; Ma and Zhang, 2020; Wang et al., 2019c). Even under the conditions of a significant decrease  
91 in air pollutant emissions, similar to the COVID-19 lockdown period, PM2.5 pollution events still  
92 occur frequently in the 28 pollution channel cities due to the unfavorable meteorological  
93 background (Shi and Brasseur, 2020; Le et al., 2020; Huang et al., 2020b; Wang et al., 2020b; Wang  
94 and Zhang, 2020b). Many studies have been conducted and have suggested that multiple  
95 meteorological factors influence the emission of primary pollutants, the formation of secondary  
96 particles and the processes of transport, accumulation and deposition of particles (Zhao et al.,  
97 2020a; Huang et al., 2020c; Chen et al., 2019; Gong and Liao, 2019). High temperatures result in  
98 greater emissions of PM2.5 precursors and secondary pollutants, and promotes photochemical  
99 reactions, causing an increase in local PM2.5 concentrations (Zhang, 2017; Zhao et al., 2018b; Chen  
100 et al., 2020). Humidity strongly affects PM2.5 concentrations in China, especially during severe  
101 pollution episodes (Zhao et al., 2018a; Li et al., 2018a; Huang et al., 2020a). Higher humidity is

102 beneficial for the hygroscopic increase in aerosols and facilitates the formation of secondary  
103 particles (Wang et al., 2019b;Zhao et al., 2017;Cheng et al., 2015;Xin et al., 2016). The cross-  
104 regional transport and horizontal diffusion of pollutants are strongly determined by the wind field.  
105 Southerly winds bring higher concentrations of air pollutants and more moisture, which enhances  
106 the local air pollution in Beijing and the surrounding regions (He et al., 2020;Zhao et al., 2020b). In  
107 addition to individual meteorological variables, synoptic circulation characteristics control the  
108 formation and development of air pollution events (Wang et al., 2020a;Miao et al., 2020;Wang and  
109 Zhang, 2020a; Liu et al., 2019). Monsoonal flows and cold frontal passages are the dominant  
110 meteorological modes controlling the day-to-day variations in PM<sub>2.5</sub> concentrations in the northern  
111 China (Li et al., 2016;Wu et al., 2017;Zhang et al., 1996;Leung et al., 2018). [Circulation of a strong  
112 Siberian High to the north and cold anomalies in the low-level troposphere with strong East Asian  
113 Trough is found to be favorable for the clear winter in Beijing and surrounding region \(Pei and Yan,  
114 2018\)](#). Weak synoptic patterns with high-pressure or persistent low-pressure systems favor the  
115 accumulation of pollutants, while, strong synoptic patterns with large pressure gradients encourage  
116 the diffusion of pollutants (Cai et al., 2020;Zhang et al., 2017;Zhang et al., 2020;Li et al., 2019).  
117 Severe haze events in the BTH region are always accompanied by stagnant air conditions, stable  
118 stratification, weak surface wind, low boundary layer height (BLH), and high relative humidity (Ma  
119 et al., 2020;Bi et al., 2014;Wang et al., 2020c;Tang et al., 2016a;Quan et al., 2020;Pei et al.,  
120 2020;Guo et al., 2019).

121 Most of the aforementioned studies focused on the synoptic pattern characteristics favorable for the  
122 initiation and development of air pollution episodes in the BTH region. During the developing phase  
123 of each PM<sub>2.5</sub> pollution episode, the comprehensive effects of secondary aerosol formation,  
124 hygroscopic increase and accumulation of particles lead to an increase in local PM<sub>2.5</sub>  
125 concentrations, which usually takes several days from a clean situation to the outbreak of a heavy  
126 haze (Sun et al., 2014;Wang et al., 2016;Pei et al., 2018). Both atmospheric chemistry and physics  
127 processes play important roles in the developing phase of air pollution events (Gu et al., 2020;Yao  
128 et al., 2018;Wang et al., 2018;Wang et al., 2010;Li et al., 2017;Gao et al., 2017). However, compared  
129 to the developing phase, which typically features a smooth increase in air pollutant concentrations  
130 [due to the regional transport, local accumulation and secondary formation](#), the decay phase of each  
131 pollution episode shows a sharp decrease in PM<sub>2.5</sub> concentrations, often in a few hours. [Pollutants  
132 on hazy days show mass concentration 2-3 times higher than that on clear days \(Li et al., 2010\)](#). The  
133 abrupt decrease in PM<sub>2.5</sub> concentrations is purely meteorological in origin and is controlled by the  
134 passage of synoptic systems, especially cold fronts, which terminate a severe air pollution episode  
135 in the BTH region by strong winds (Zhu et al., 2016;Jia et al., 2008;Ji et al., 2012;Xin et al., 2012).  
136 [Many studies took the smooth increase period of PM<sub>2.5</sub> concentrations and abrupt decrease stage](#)

137 following it as a complete air pollution episode, and investigate its development mechanism (Tang  
 138 et al., 2016b; Zhang et al., 2018b; Sun et al., 2014; Zheng et al., 2015). However, it is still unclear  
 139 how strong the wind needs to be, exactly what kind of synoptic systems can effectively terminate  
 140 air pollution episodes in the BTH region, and what mechanism is responsible for the rapid reduction  
 141 in PM2.5 concentrations in a few hours. The clarification of these issues will contribute to  
 142 improving local air quality predictions. The variation in air quality is generally consistent in the 28  
 143 pollution channel cities, especially in the decay phase of pollution episodes, which indicates that  
 144 the same synoptic system usually affects the whole region. This study will focus on the region  
 145 covering these 28 pollution channel cities and reveal the synoptic circulation pattern that dominates  
 146 the decay process of PM2.5 pollution events.

## 147 2. Data and Method

### 148 2.1 Dataset

149 The daily mean observed PM2.5 concentrations in the 28 pollution channel cities from January 2014  
 150 to March 2020 were obtained from the Ministry of Ecology and Environment of the People's  
 151 Republic of China (<https://www.aqistudy.cn/historydata/>). Fig. 1 shows the location of the 28  
 152 pollution channel cities and their annual mean PM2.5 concentrations from 2014 to 2019. The four-  
 153 times-daily dataset of the fifth-generation European Centre for Medium-Range Weather Forecasts  
 154 (ECMWF ERA5) atmospheric reanalysis dataset with a resolution of 0.5°  
 155 (<https://cds.climate.copernicus.eu/cdsapp#!/dataset/10.24381/cds.bd0915c6?tab=form>) was used to  
 156 describe the meteorological characteristics and synoptic circulation classification. Daily  
 157 accumulated precipitation amount is the total amount of 24-hour values.

158 The divergence of local PM2.5 flux can be taken as a metric for the PM2.5 budget in a specific  
 159 region, with positive divergence indicating net outflow of air pollutants from the domain region,  
 160 and vice versa. The daily mean divergence of the PM2.5 flux over the region of 34-40° N and 112-  
 161 118° E is calculated according to Eq.(1):

$$162 \quad D = D_z + D_m = \frac{\partial}{\partial x}(UQ) + \frac{\partial}{\partial y}(VQ) = \sum_{i=1}^n \frac{(U_{Ei}Q_{Ei} - U_{Wi}Q_{Wi})}{2\Delta X} + \sum_{j=1}^m \frac{(V_{Nj}Q_{Nj} - V_{Sj}Q_{Sj})}{2\Delta Y} \quad (1)$$

163 where  $D_z$  and  $D_m$  are the zonal and meridional components of the net divergence of PM2.5 flux for  
 164 the specific region. The parameters  $n$  and  $m$  indicate the meridional and zonal grid numbers of the  
 165 domain. The subscripts  $E$  and  $W$  mark the variables at the longitudes of the eastern and western  
 166 boundaries of the domain. Similarly, the subscripts  $S$  and  $N$  represent the values at the latitudes of  
 167 the southern and northern boundaries.  $U_{Ei}$  (units in m/s) indicates the 10 m zonal wind in the  $i$ th grid

删除的内容: the

169 of the eastern boundary of the domain.  $Q_{Nj}$  (units in  $\mu\text{g}/\text{m}^3$ ) is the spatially interpolated PM2.5  
170 concentration in the  $j$ th grid at the latitude of the northern boundary.  $\Delta X$  and  $\Delta Y$  represent the zonal  
171 and meridional distance of each grid (units in meters). Due to the limited information on the vertical  
172 distribution of PM2.5 and the horizontal winds are closely related with PM2.5 concentration as  
173 revealed by previous studies, the horizontal divergence of PM2.5 flux is used to evaluate the net  
174 inflow and outflow of local air pollutants in this study.

## 175 2.2 Thresholds for the decay process of air pollution episodes

176 Fig. 2 shows the daily PM2.5 concentration variations of the 28 pollution channel cities from  
177 January to March 2019. PM2.5 concentrations exhibit a recurring smooth increase followed by a  
178 sharp decrease, which is known as a sawtooth cycle (Jia et al., 2008). During the developing phase  
179 of each pollution episode, the PM2.5 concentrations show the same smoothly increasing trend with  
180 slight differences in the increase rate in the 28 pollution channel cities (i.e., an average increase  
181 trend of  $10.37 \pm 42.2 \mu\text{g}/(\text{m}^3 \cdot \text{day})$  during January to March 2019). The inhomogeneity of the  
182 PM2.5 concentration increase in the 28 cities, indicating by the large standard deviation of increase  
183 trends (approximate four times the magnitude of increase trend), may be due to the complicated  
184 physiochemical processes of haze formation. By contrast, as shown by dotted lines in Fig. 2,  
185 regional synchronous decreases in PM2.5 concentrations occur in the decay phase of pollution  
186 episodes with an average trend of  $-50.06 \pm 46.83 \mu\text{g}/(\text{m}^3 \cdot \text{day})$ . Most of the consistent  
187 improvements in air quality in the decay phase can be attributed to the effects of the synoptic system.  
188 Therefore, in this study, if more than 40% of the 28 pollution channel cities with the day-to-day  
189 PM2.5 concentrations decreased by 30% (relative to the value of the previous day) or more than 60%  
190 of the channel cities with PM2.5 concentrations decreased by 30% in two successive days, it can be  
191 defined as the occurrence of the decay phase of pollution episodes. If two consecutive days were  
192 defined as the decay phase, only the first day was selected be valid and retained. In total, 365 days  
193 are identified as the decay phase of pollution episodes from January 2015 to March 2020 (see Fig.  
194 4) and are used for the synoptic pattern classification.

## 195 2.3 Method of synoptic circulation classification

196 The T-mode principal component analysis (PCA) method was used to objectively classify the type  
197 of synoptic system dominating the decay phase of pollution episodes, as this method has an  
198 outstanding performance in terms of the reproduction of predefined types and temporal-spatial  
199 stabilities (Huth et al., 2008; Cavazos, 2000; Tie et al., 2015; Valverde et al., 2015; Xu et al., 2016).  
200 The T-mode PCA has been widely used to investigate the general circulation patterns, climate  
201 change and air quality and has been incorporated into the European Cooperation in Science and

删除的内容: rate of

删除的内容: and magnitude

删除的内容: i

删除的内容: ed

206 Technology (COST) plan 733 toolbox (COST733: <http://cost733.geo.uni-augsburg.de/cost733wiki>)  
207 (Philipp et al., 2014). The daily mean geopotential height (Z), U and V components at 925 hPa on  
208 the 365 decay phase days are used for synoptic pattern classification. To exclude the effects of  
209 seasonal variation on atmospheric circulation and to ensure that different synoptic patterns in the  
210 same season are comparable, the T-mode PCA method is applied to the four seasons respectively.  
211 The target region is 32-44° N and 110-122° E, as shown in Fig. 1. For each season, the three input  
212 data matrixes (U, V and Z) have temporal and spatial dimensions, with spatial grids and time series  
213 represented by rows and columns, respectively. To speed up computations of the T-mode PCA in  
214 the COST733 toolbox, each matrix is first divided into 10 subsets. Then, the principal components  
215 (PCs) are determined using the singular value decomposition for each subset, and an oblique  
216 rotation is applied to the PCs to achieve better classification effects. The 10 classifications based on  
217 the subsets are evaluated by the chi-square test and the subset with the highest sum is selected and  
218 assigned to a type.

219 The Lamb-Jenkinson-Collison type classification (JCT) is also a widely adopted method to identify  
220 synoptic circulation pattern by describing the location of cyclonic/anticyclonic centers and the  
221 direction of the geostrophic flow (Li et al., 2020;Fan et al., 2015;Jiang et al., 2020;Chen,  
222 2000;Jenkinson and Collison, 1977). In order to verify the robust of circulation classification results  
223 of PCA method, JCT method is also involved based on daily mean gridded sea level pressure at 16  
224 points centered by 37° N and 117° E as shown in SI. According to Fig. S1 and Fig. S3, it shows  
225 similar circulation pattern of PAC and JCT method, indicating the consistence of the two  
226 classification methods. Because JCT method is specialized on classifying daily mean sea level  
227 pressure patterns, which will ignore the thresholds of some other meteorological variables to some  
228 extent (Philipp et al., 2014). Therefore, we only focus on the results of PCA hereafter.

## 229 3. Results

### 230 3.1 Identification of the occurrence of the decay process of air pollution episodes

231 The magnitude of the day-to-day variation in PM<sub>2.5</sub> concentrations is an important metric for  
232 recognizing the occurrence of the decay phase of air pollution. Fig. 3 shows the frequency of the  
233 relative day-to-day PM<sub>2.5</sub> concentration differences in the 28 pollution channel cities during the  
234 period of January 2014 to March 2020. Table 1 summarizes the occurrence frequency of the day-  
235 to-day PM<sub>2.5</sub> differences in the specific segment. It shows that a fatter-tailed probability distribution  
236 exists in winter than in summer; thus, winter features a lower probability of weak PM<sub>2.5</sub> variations  
237 and a higher probability of strong PM<sub>2.5</sub> variations, indicating greater day-to-day variability in

238 PM2.5 concentrations. In winter, 8.6% of PM2.5 concentrations decreased by over 60%, and 14.9%  
239 increased by more than 80%, whereas, in summer, the values were only 2.4% and 6.6%. A total of  
240 38.3% of the cases show day-to-day PM2.5 variations within the range of -20% to 40% in winter,  
241 but where a total of 55.6% is observed in summer. The PM2.5 variations in spring and autumn  
242 exhibit almost the same distribution patterns, with a relatively higher frequency of strong PM2.5  
243 variations in autumn. Generally, the probability distributions in spring and autumn are between  
244 those of summer and winter. The stronger day-to-day decreases in PM2.5 concentrations,  
245 particularly the sharp wintertime reductions, may be attributable to the passage of a cold front  
246 synoptic system, and the results suggest that the winter PM2.5 variations are the most sensitive to  
247 synoptic patterns.

248 According to the occurrence of day-to-day PM2.5 differences in the 28 pollution channel cities, i.e.,  
249 thresholds for the decay phase of air pollution episodes in Section 2.2, 365 decay processes have  
250 been recognized from January 2014 to March 2020. If the daily mean accumulated precipitation  
251 amount is more than 1 mm for all the grid cells in the region of 36°-42° N and 113°-117.5° E  
252 (covering the 28 cities), the specific day is defined as a rainy day with effective wet deposition. 97  
253 of the 365 decay phases are defined as rainy days, in which case the abrupt decrease in ambient  
254 PM2.5 concentrations are assumed to be related to wet deposition. Only the decay processes on dry  
255 days are involved in the synoptic pattern classification in the following work. Figure 4 shows the  
256 annual cycle of the decay process frequencies in a specific year. In most years, the figure shows a  
257 two-peak annual cycle of the decay phase frequency with a valley in summer, and the valley  
258 becomes deeper after removing the rainy cases. There are 105 (105), 62 (21), 86 (56) and 112 (109)  
259 decay process days in spring, summer, autumn and winter for all (dry-day) cases, respectively.  
260 Approximately 70% of the regional sharp reduction in summer can be attributed to the effect of wet  
261 deposition.

### 262 3.2 Classification of the synoptic circulation dominating the decay processes of air pollution 263 episodes

264 T-mode PCA circulation classification has been applied to the dry-day decay process in individual  
265 seasons. Fig. S1 and Fig. 5 show the original and anomalous circulation patterns at 925 hPa under  
266 each circulation type (CT) condition. Two dominant circulation types (CTs) are identified in summer.  
267 Three CTs are identified for each of the other seasons, respectively. The three dominant CTs in  
268 spring show almost the same pattern as those of autumn and winter, and only the occurrence  
269 frequency of the CTs differ among the seasons. The strong prevailing northwesterly wind in the CT2  
270 condition is the commonly accepted synoptic circulation favorable for the rapid decay of pollution  
271 episodes in the BTH region, and CT2 is also the most frequent CT for the decay phase in autumn

刪除的內容: have effective precipitation more than of 10 mm/day,

刪除的內容: the

刪除的內容: s

刪除的內容: 5

刪除的內容: 6

刪除的內容: ,

刪除的內容: and

刪除的內容: t

刪除的內容: in the

282 and winter. A large-scale high-pressure system covers the region of central-western Mongolia,  
 283 northern Xinjiang, Inner Mongolia and Shaanxi Province in China. Deep low pressure is situated in  
 284 the northeastern China and northern Japan. The BTH region is located between the east of the  
 285 anticyclone and west of the cyclone, and is dominated by strong northwesterly surface winds with  
 286 the speeds of 2.98~3.88 m/s in different seasons. The northwesterly wind corresponds to the  
 287 significant northerly wind anomaly, which is beneficial for the transport of cold, clean and dry air  
 288 masses southward. Although it shows downward motion due to the upper westerly wind passing the  
 289 leeward side (see Fig. 6), the other meteorological variables summarized in Fig. 7 reveal that the  
 290 highest wind speed, the highest boundary layer height (BLH) and the lowest relative humidity occur  
 291 under CT2 conditions, all of which are favorable for the reduction of PM2.5 concentrations. Fig. 8  
 292 and Fig. S4 exhibits the distribution of PM2.5 flux divergence over the region of 34-40° N and 112-  
 293 118° E, and its zonal and meridional components, with positive divergence indicating net horizontal  
 294 outflow of air pollutants from the BTH region, and negative divergence indicating the opposite. The  
 295 PM2.5 flux divergence is found to have significantly positive values in most of CTs, indicating that  
 296 the local ambient PM2.5 concentrations decrease with the horizontal removal of the polluted air  
 297 mass or the replacement by clean air. As shown in Fig. S4, the positive divergence of the PM2.5  
 298 flux in CT2 is mainly contributed by the significant outflow of air pollutants from eastern and  
 299 southern edges. Clean, dry and strong northwesterly winds in the CT2 condition are the major  
 300 drivers of the decay process of air pollution episodes.

301 For CT1 in spring, autumn and winter, a surface high-pressure system initiates from the Siberian  
 302 region and slants forward to central Inner Mongolia and the BTH region, resulting in a position that  
 303 is more northeastward than the anticyclonic circulation in CT2 (Fig. S1). Most areas in China are  
 304 controlled by a high-pressure system. The BTH region is located on the southeastern edge of the  
 305 anomalous anticyclone, and dominated by a remarkable northeasterly wind anomalies. The average  
 306 surface wind speed is of 2.63~3.02 m/s, which is higher than the seasonal mean but not as high as  
 307 that under CT2 conditions. Although all the surface wind speed, BLH and relative humidity show  
 308 favorable patterns for air pollutant diffusion under CT1 conditions, the magnitudes of the above  
 309 anomalies are not as significant as those under CT2 conditions. Therefore, there must be other  
 310 mechanisms responsible for the decay process of pollution episode that are distinct from those of  
 311 CT2, as is generally believed. The northeasterly wind anomaly brings clean and dry air masses to  
 312 the BTH region, and increases the outward and southward transport of local air pollutants in the  
 313 meanwhile, which results in the negative relative humidity anomaly shown in Fig. 7. The net  
 314 divergence of air pollutants (i.e., positive divergence of the PM2.5 flux in Fig. 8) is the most  
 315 significant under CT1 conditions, indicating the contribution of horizontal transport to the rapid  
 316 decay of pollution episodes. The net outflow of pollutants is attributed to the significant positive

删除的内容: 7

删除的内容: 8

删除的内容: 9

删除的内容: all three

删除的内容: with

删除的内容: T

删除的内容: the meridional outflow, which highlights the effects of the northerly wind anomaly.

删除的内容: In

删除的内容: within

删除的内容: high-pressure center with an anticyclonic horizontal wind shear in the domain

删除的内容: high

删除的内容: According to the anomaly pattern in Fig. 6, the BTH region is located at the south of the anticyclone, which is dominated by a remarkable northeasterly wind anomaly. This

删除的内容: 8

删除的内容: 9



336 divergence of PM2.5 flux in the southern edge (Fig. S4). In terms of vertical anomalous circulation,  
337 the BTH region is located under the east of a high-level ridge and west of a high-level trough (Fig.  
338 S5), where there is often upper-level convergence and cause the surface high-pressure anomaly to  
339 get higher (see Fig. 5). The upper level convergence leads to the vertical sinking in the east of the  
340 BTH region, which also delivers upper dry and clean air to the surface. In addition, as shown in Fig.  
341 6, the significant clean vertical sinking airflow in the east of the BTH region combined with the  
342 surface easterly wind anomaly results in air movement westward across the domain and climbs up  
343 along the western mountain region. The upward flow carries the near-surface air pollutants to the  
344 upper level of the boundary layer, where the pollution quickly spreads to the free atmosphere due  
345 to the effective entrainment caused by the strong wind shear at the top of the boundary layer (see  
346 Fig. 6). In general, the remarkable horizontal net-outflow of air pollutants, negative humidity  
347 anomaly and effective outward spread of air pollutants to the free atmosphere promote the abrupt  
348 reduction of local PM2.5 concentrations.

349 CT3 is the dominant synoptic pattern for the decay process in spring, with the highest frequency of  
350 47%, compared with frequencies of 30% and 17% in autumn and winter. In this kind of circulation  
351 pattern, there is only a closed low-pressure system located over the northeastern China, with large  
352 pressure gradients around the cyclone and weak gradients over most parts of China (Fig. S1). The  
353 BTH region borders the cyclone system to the northeast, which leads to a prevailing westerly wind  
354 with speeds of 2.29–3.07 m/s. The low-pressure and westerly wind features are more significant  
355 based on the anomalous circulation in Fig. 5, especially in winter. As shown in Fig. S5, a deep  
356 trough persists in the northern BTH region in 500 hPa, bringing cold air masses from the northwest.  
357 According to the distribution of 24 h backward trajectories of Beijing in Fig. S6, the northwesterly  
358 cold and dry air mass are taking to the domain, benefiting for the decay of local pollution episodes.

359 Similar to CT1 and CT2, negative relative humidity anomalies and positive surface wind speed  
360 anomalies are also favorable for the decay of pollution episodes. Given the distribution of the BLH,  
361 there is no significant positive anomaly signal in CT3, unlike in CT1 and CT2. Although a moderate  
362 BLH is observed under CT3 conditions, strong vertical wind shear occurs near the surface, as shown  
363 in Fig. 6, which results in more uniform vertical distribution of air pollutants in the boundary layer.  
364 Moreover, obvious horizontal PM2.5 divergence also provides a possibility for the decay of air  
365 pollution episodes. To be more precise, the zonal divergence of the PM2.5 flux that dominates the  
366 net divergence of the whole region, rather than the meridional component as the other two  
367 circulation patterns (Fig. 8 and Fig. S2). The inflow of clean and dry air masses combined with the  
368 good performance of boundary layer mixing are the main reasons for the immediate improvement  
369 of air quality when CT3 occurs.

370 In terms of the synoptic patterns in summer, two CTs are classified excluding the effects of wet

删除的内容: y

删除的内容: figure not shown here

删除的内容: 2

删除的内容:

带格式的: 非 突出显示

删除的内容: 6

删除的内容: 7

删除的内容: 7

删除的内容: at 925 hPa

删除的内容: 6

带格式的: 非 突出显示

删除的内容: 2

删除的内容: In the upper 500 hPa,

删除的内容: 7

删除的内容: improves

删除的内容: the

385 deposition. According to the circulation anomaly in Fig. 5, the synoptic pattern of CT1 in summer  
386 is similar to that of CT3 at 925 hPa in other seasons, which is dominated by a northeastern cyclonic  
387 circulation. Dry northwesterly wind occurs in the BTH region, reducing the local relative humidity.  
388 As shown in Fig. 7, the BLH is higher than the seasonal average, indicating an increase in vertical  
389 diffusion space. The zonal positive divergence of the PM2.5 flux is offset by the negative value in  
390 the meridional direction. The effect of horizontal transport of air pollutants can be ignored in this  
391 situation. Therefore, the decay process of the air pollution episode in the CT1 condition can be  
392 attributed to the dry air mass and higher than normal BLH.

删除的内容: 6

393 In the anomaly pattern of the CT2 condition in summer, the BTH region is located between the  
394 southern portion of a high-pressure system and the northern portion of a low-pressure system, and  
395 is affected by the prevailing northeasterly surface wind. Clean air masses are transported to the BTH  
396 region along with the northeasterly wind, which can be confirmed by the positive divergence in the  
397 PM2.5 flux in both zonal and meridional directions. Both the negative relative humidity and positive  
398 BLH anomalies in CT2 are beneficial for the reduction of surface PM2.5 concentrations, but the  
399 magnitude of the anomaly is not as high as those of the CT1 condition. There is no favorable signal  
400 for the diffusion of surface PM2.5 in terms of the vertical motion in the two synoptic patterns in  
401 summer. It is the effective horizontal outflow that promotes the decay process of pollution episodes.

删除的内容: 8

### 402 3.3 Synoptic circulation effects on the PM2.5 pollution

403 Section 3.2 shows different physical mechanisms for the rapid decay of air pollution episodes in the  
404 region covering the 28 pollution channel cities. Fig. 9 exhibits the relative difference in PM2.5  
405 concentrations between the day before and after the occurrence of the specific synoptic CTs. The  
406 average PM2.5 differences in the 28 pollution channel cities are summarized in Table 2.  
407 Unsurprisingly, it shows a remarkable decrease in PM2.5 concentrations when all the circulation  
408 patterns dominate the decay process occurs, but it is worth noting that the magnitudes of the decline  
409 vary according to the synoptic patterns. For the case of spring, autumn and winter, CT2 conditions  
410 demonstrate the most significant effects on the abrupt reduction in PM2.5 concentrations, with a  
411 more than 40% day-to-day decrease in PM2.5 concentrations in the 28 pollution channel cities in  
412 all three seasons. CT1 conditions are second in terms of the circulation influence in the decay  
413 process of PM2.5 pollution episodes. The PM2.5 concentrations decrease quickly by 37.2%, 40.1%  
414 and 36.9% when CT1 conditions occur in spring, autumn and winter, respectively. The CT3  
415 conditions, which are dominated by westerly winds, show a relatively weak ability on control the  
416 decay process of PM2.5 pollution episodes. Air quality improves by approximately 26~29%  
417 compared with the previous day due to the occurrence of CT3 conditions. In summer, PM2.5  
418 concentrations decrease more significantly with the occurrence of CT1 conditions than with the

删除的内容: 10

422 occurrence of CT2 conditions, indicating more effective diffusion under northwesterly winds than  
423 under northeasterly airflow. Wet scavenging is an effective method for the rapid decay of air  
424 pollution episodes, especially in wintertime. PM2.5 concentrations drop sharply after the occurrence  
425 of precipitation, with decreases of more than 35% in spring, autumn and winter. 26.2% of PM2.5  
426 pollution is removed by the wet deposition in summer, which is the lowest rate among the four  
427 seasons. The relatively clean background may account for the weak wet deposition effects in  
428 summer.

429 Fig. 2 shows the sawtooth cycle variation in PM2.5 concentrations with a smooth increase followed  
430 by an abrupt decrease. However, the PM2.5 concentrations do not always increase gradually before  
431 the decay of the pollution episode. Here, the sawtooth cycle is divided into developing and decay  
432 phases, and the interval stage between two decay phases is defined as the developing phase of a  
433 specific pollution episode. As shown in Fig. 10, when the duration of the developing phase is less  
434 than 3-days, air pollutants accumulate gradually to a maximum until the occurrence of decay process  
435 occurs. However, if the developing phase is longer than 3-days, the highest PM2.5 concentrations  
436 occur on 1-3 days before the passage of a favorable synoptic system, which indicates that the  
437 developing mature stage of pollution episodes (with high level concentrations) usually persist for  
438 several days.

439 The duration of the developing phase not only changes the shape of the sawtooth cycle but also  
440 affects the maximum PM2.5 concentrations during the pollution episode, as shown in Fig. 11. Most  
441 of the durations of the developing phase are concentrated in the period of shorter than 5-days in  
442 spring, autumn and winter, with average durations of 5.53, 5.86 and 5.36 days, respectively. As the  
443 main wave system affecting the synoptic circulation in mid-latitude region, the Rossby wave has  
444 about one-week cycle length, which dominates the average duration of two adjacent decay phase.  
445 Typically, for the cases in spring and autumn, when the durations are less than 5 days, the maximum  
446 PM2.5 concentrations during the specific air pollution episode increase with an increase in the  
447 developing phase durations; but the concentrations remain unchanged if the duration longer than 5  
448 days. In winter, the maximum PM2.5 concentrations in a specific sawtooth cycle continue to  
449 increase with increases in the interval between two decay processes. Wintertime air pollution can  
450 be exacerbated by the long-term absence of an effective decay process. The frequency of favorable  
451 circulation patterns is relatively lower in summer, which leads to an effective decay process  
452 occurring every 7.45 days. The maximum PM2.5 concentrations display an upward tendency with  
453 increases in the developing stage durations, but there are some small fluctuations in the mean value  
454 of the highest PM2.5 concentration due to the limited samples in summer.

455 Emission and meteorological elements are taken as the two most important factors controlling the

删除的内容: 1

删除的内容: 2

458 variation in PM2.5. Many efforts have been made to mitigate the air pollutant emissions in the 28  
459 pollution channel cities, which have achieved remarkable improvements in air quality in recent  
460 years. However, because obvious interannual difference of the meteorological conditions are  
461 observed, there is uncertainty in the evaluation of emission reductions based on the observed PM2.5  
462 concentrations. The quantitative evaluation of the effects of emission reduction measures on the  
463 PM2.5 concentration variation has been a challenge for policy makers and stakeholders. Here, only  
464 the PM2.5 concentrations observed on the days of decay processes are compared, which excludes  
465 the different effects of meteorological conditions and evaluates the pure effects of emission  
466 reduction from a certain perspective. Fig. 12 shows a significant decline in seasonal mean PM2.5  
467 concentrations from 2014 to 2020 in the 28 pollution channel cities. This figure shows almost the  
468 same rates of decrease in all four seasons, with relatively smaller decreases of 4.8 and 4.3  $\mu\text{g}/(\text{m}^3 \cdot \text{yr})$   
469 in spring and winter and greater decreases of 5.7 and 5.2  $\mu\text{g}/(\text{m}^3 \cdot \text{yr})$  in summer and autumn,  
470 respectively. The slight difference in the seasonal decreasing tendency is possibly due to seasonal  
471 difference in the main sources of air pollutant emissions.

删除的内容: 3

删除的内容: also

删除的内容: differen

删除的内容: ce

#### 472 4. Conclusions and Discussion

473 The variation in ambient air pollutant concentrations generally represents a continuous sawtooth  
474 cycle with a recurring smooth increase followed by a sharp decrease. The combined effects of  
475 emissions, secondary formation of particles and unfavorable meteorological conditions trigger the  
476 initiation and development of a specific PM2.5 pollution episode over several days. In contrast, the  
477 abrupt decay of a pollution episode is mostly due to the passage of favorable synoptic patterns, and  
478 it usually takes a few hours transition from hazy to clean air condition. The detailed atmospheric  
479 circulation features and the mechanisms through which they affect the decay processes of pollution  
480 episodes are discussed in this work. A total of 365 decay processes were recognized from January  
481 2014 to March 2020 based on the regional variation in the day-to-day PM2.5 concentration  
482 difference. 97 of the 365 decay phases were related to the effective wet deposition, and most of  
483 them occurred in summer. For the dry-day decay processes, 105, 21, 56 and 109 cases occurred in  
484 spring, summer, autumn and winter, respectively. The intervals between two continuous decay  
485 processes are 5.53, 7.45, 5.86 and 5.36 days from spring to winter, respectively, which may be  
486 controlled by the cycle length of Rossby waves in the mid-latitude region.

删除的内容: that

删除的内容: the

删除的内容: s

删除的内容: s

删除的内容: for conditions to

删除的内容: A relatively fatter-tailed probability distribution of day-to-day PM2.5 concentration over the 28 pollution channel cities is observed in winter compared with summer, indicating that winter features a lower probability of weak PM2.5 variations and a higher probability of strong PM2.5 variations. The probability distribution of day-to-day PM2.5 variations in spring and autumn lies between those of summer and winter.

487 All the CTs are common in positive wind speed anomaly, negative relative humidity anomaly and  
488 effective outflow of PM2.5 from the domain. Although the magnitude and significance of the  
489 anomalies are different in the specific CT, all the above variables indicate favorable atmospheric  
490 diffusion conditions, which is benefit for the decay of pollution episodes. There are also some

508 prominent features for each CT. In CT1, the most significant horizontal outflow of air pollutants  
509 combining with the upward transport of airflow to the free atmosphere are the two extra drivers for  
510 the decay processes. The removal efficiency of CT1 is 35-40%, which is moderate among the three  
511 CTs. In terms of CT2, it is the most frequent CT in autumn and winter. The circulation with the  
512 heaviest wind speed from the northwest, the highest BLH, lowest relative humidity jointly results  
513 in the quickly decrease in PM2.5 concentration in a few hours, which is the commonly accepted  
514 circulation feature to terminate the severe pollution episodes. Due to the significantly favorable  
515 meteorological conditions, CT2 has the strongest cleaning abilities of 41-45% in different seasons.  
516 For CT3, the synergy effects of enhanced vertical mixing within the boundary layer and moderate  
517 beneficial background of wind speed, relative humidity and horizontal divergence of PM2.5 are the  
518 main cleaning mechanism of CT3 condition. After the passage of CT3, 26-29% of local air  
519 pollutants are typically removed. The two dry-day circulation patterns in summer are similar to the  
520 synoptic patterns of CT1 and CT3 in the other three seasons. A dry air mass with a positive BLH  
521 anomaly and the effective horizontal outflow of air pollutants are the main reasons for the abrupt  
522 decay phases in summer. The average PM2.5 concentrations on decay process days show a  
523 significant decreasing trend from 2014 to 2020, which indicates the success of emission mitigation  
524 efforts. Emission reductions have led to a 4.3-5.7  $\mu\text{g}/(\text{m}^3 \cdot \text{yr})$  decrease in PM2.5 concentrations in  
525 the 28 pollution channel cities.

526 Due to the limitation of dataset about PM2.5 vertical distribution, only the horizontal  
527 divergence of PM2.5 flux is used in this study. Although it shows positive divergence for all of  
528 the CTs, indicating the remarkable contribution of the net outflow of air pollutants at the surface  
529 to the quickly decrease in PM2.5 concentrations, the effects of horizontal PM2.5 flux above the  
530 surface or the vertical diffusion cannot be neglected, which may have great contribution in a  
531 specific event, and need to be further studies. PM2.5 concentrations sharply decrease after the  
532 passage of CT2, but it shows a relatively weak drop in air pollutant concentrations when CT3  
533 occurs, which can be attributed to its moderate strength of anomalies circulation pattern.  
534 Therefore, the scavenging effects of each CT should also be taken into account when predicting  
535 the air quality based on synoptic circulation variation.

536 **Code/Data availability:** Daily PM<sub>2.5</sub> concentration observations at the 28 channel cities were  
537 obtained from the website of Ministry of Ecology and Environment of the People's Republic of  
538 China (<http://106.37.208.233:20035>). Daily four times ECMWF ERA5 dataset during 2014 to 2020  
539 are downloaded from <https://www.ecmwf.int/en/forecasts/datasets/reanalysis-datasets/era5>.  
540 Atmospheric circulation classification was conducted using European Cooperation in Science &  
541 Technology (COST) plan 733 (cost733class software), which can be downloaded at  
542 <http://cost733.met.no>.

删除的内容: . . .  
Due to the limitation of dataset about PM2.5 vertical

545

546 **Author contributions:** XW and RZ designed research. XW, YT and WY performed the analyses  
547 and wrote the paper. All authors contributed to the final version of the paper.

548

549 **Competing interests:** The authors declare that they have no conflict of interest.

550

551 **Acknowledgements:** We thank the support of Fudan University-Tibet University Joint Laboratory  
552 For Biodiversity and Global Change. This research has been funded by the National Natural Science  
553 Foundation of China (grant nos. [41805117](#), [42075058](#), [41975075](#) and [41790470](#)).

554

### 555 **Figure captions:**

556

557 [Figure 1. Distribution of annual mean PM2.5 concentrations in the 28 cities by altitude. The PM2.5](#)  
558 [concentration is the annual mean value from 2014 to 2019 \(units:  \$\mu\text{g}/\text{m}^3\$ \). The elevation over the](#)  
559 [domain was obtained from Global Digital Elevation Model with a resolution of  \$0.5^\circ \times 0.5^\circ\$ .](#)

560

561 **Figure 2.** Time series of daily mean PM2.5 concentrations in the 28 pollution channel cities from  
562 January to March 2019 (units:  $\mu\text{g}/\text{m}^3$ ).

563

564 **Figure 3.** Probability distribution of the relative day-to-day difference of PM2.5 concentrations. The  
565 relative difference is based on the PM2.5 concentration on the previous day. The distributions in  
566 spring and autumn are combined in the upper panel, and cases in winter and summer are shown at  
567 the bottom.

568

569 **Figure 4.** Monthly cumulative occurrence of the decay processes of pollution episodes. The orange  
570 curve indicates the decay process occurrences on dry days. In total, 365 decay processes are  
571 identified from January 2014 to March 2020, and 97 of them are associated with precipitation levels

删除的内容: , 41805117 and 41975075

删除的内容: Figure 1. Annual mean PM2.5 concentrations in the 28 pollution channel cities of Beijing from 2014 to 2019 (units:  $\mu\text{g}/\text{m}^3$ ). . .

576 greater than 10 mm/day.

577

578 Figure 5. Distribution of the geopotential height anomalies (shaded, unit:  $m^2/s^2$ ) and wind field  
579 anomalies at 925 hPa for each circulation type. The number over each subplot indicates the  
580 occurrence frequency of the specific circulation type. The solid blue box is the location of the  
581 domain region covering the 28 pollution channel cities.

582

583 Figure 6. Zonal averaged profile of the distribution of vertical wind shear anomalies in the domain  
584 region (shaded, units:  $m/(s \cdot 100 m)$ ) and the vertical and zonal circulation anomalies. The green line  
585 indicates the average location of the top of the boundary layer. Zonal wind shear, circulation and  
586 boundary layer height are the average values between 34-40° N. The two dashed lines are the eastern  
587 and western boundaries of the domain (112 to 118° E). The grey region indicates the average altitude  
588 between 34-40° N.

589

590 Figure 7. Boxplot of surface wind speed, boundary layer height (BLH), sea level pressure (slp) and  
591 relative humidity (RH) for each circulation type. The dashed line indicates the seasonal mean of the  
592 specific variables. The mean values of all of the meteorological variables in each CT are  
593 significantly different with their seasonal mean based on two-tail student-t test at a significant level  
594 of 0.01.

595

596 Figure 8. Boxplot of the divergence of PM2.5 flux over the region of 34-40° N and 112-118° E. The  
597 daily divergence is calculated based on the Eq. (1). Zonal and meridional components are the first  
598 and second terms of the formula. \* in the x axis marks the divergence in a specific CT is significantly  
599 different with zero based on two-tail student-t test at a significant level of 0.01.

600

601 Figure 9. Distribution of the daily mean PM2.5 concentrations before and after the occurrence of  
602 decay processes of pollution episodes in the 28 pollution channel cities. The hollow box indicates  
603 the concentration on the decay phase day, and the solid box is the value on the previous day. The  
604 relative differences in the PM2.5 concentrations after the occurrence of decay process are  
605 summarized in Table 2. The number at the top of each box indicates the sample size used for the  
606 boxplot. The number in the first line is the sample size of the “before” case; and the second line is

删除的内容: Figure 5. Distribution of the geopotential height (shaded, units:  $m^2/s^2$ ) and wind fields at 925 hPa for each circulation type. The number over each subplot indicates the occurrence frequency of the specific circulation type. The solid blue box is the location of the domain region covering the 28 pollution channel cities.

删除的内容: Figure 6. Distribution of the geopotential height anomalies (shaded, unit:  $m^2/s^2$ ) and wind field anomalies at 925 hPa for each circulation type.

删除的内容: 7

删除的内容: Figure 8. Boxplot of surface wind speed, boundary layer height (BLH), sea level pressure (slp) and relative humidity (RH) for each circulation type. The dashed line indicates the seasonal mean of the specific variables.

删除的内容:

删除的内容: Figure 9. Boxplot of the divergence of PM2.5 flux over the region of 34-40° N and 112-118° E. The daily divergence is calculated based on the Eq.(1). Zonal and meridional components are the first and second terms of the formula.

删除的内容: 10

629 for the “after” case.

630

631 Figure 10. The day of the maximum PM2.5 concentration during each pollution episode varies with  
632 the duration of the developing phase.

删除的内容: 1

633

634 Figure 11. The density plot of the maximum PM2.5 concentration according to the duration of the  
635 developing phase of pollution episodes. Daily PM2.5 concentrations are normalized by their  
636 monthly mean value to exclude the effects of seasonal and interannual variations in air quality. A  
637 warmer color indicates a higher density of scatter. Pentagrams mark the average maximum PM2.5  
638 concentration for the specific duration period.

删除的内容: 2

639

640 Figure 12. Variations in the average PM2.5 concentration on all the decay phase days from 2014 to  
641 2020. The black hollow circles indicate the mean PM2.5 concentration in each year. The black line  
642 is the fitting line based on the montly median value. The number in the subplot is the linear trend  
643 (t), R-square and p-value of least squares regression model. \*\* after linear trend indicates the linear  
644 regression model is significant with a p-value<0.01.

645

删除的内容: Figure 13. Variations in the average PM2.5 concentration on all the decay phase days from 2014 to 2020. The black hollow circles indicate the mean PM2.5 concentration in each year. The black line is the fitting line based on the mean value. The number in the subplot is the linear trend of the fitting line. .



## 654 **References**

- 655 Bi, J., Huang, J., Hu, Z., Holben, B., and Guo, Z.: Investigating the aerosol optical and radiative  
656 characteristics of heavy haze episodes in Beijing during January of 2013, *J. Geophys. Res. Atmos.*, 119,  
657 9884-9900, 2014.
- 658 Cai, W., Li, K., Liao, H., Wang, H., and Wu, L.: Weather conditions conducive to Beijing severe haze  
659 more frequent under climate change, *Nat. Clim. Chang.*, 7, 257-262, 2017.
- 660 Cai, W., Xu, X., Cheng, X., Wei, F., Qiu, X., and Zhu, W.: Impact of “blocking” structure in the  
661 troposphere on the wintertime persistent heavy air pollution in northern China, *Sci. Total Environ.*,  
662 140325, 2020.
- 663 Cavazos, T.: Using self-organizing maps to investigate extreme climate events: An application to  
664 wintertime precipitation in the Balkans, *J. Clim.*, 13, 1718-1732, 2000.
- 665 Che, H., Xia, X., Zhao, H., Dubovik, O., Holben, B. N., Goloub, P., Cuevas Agulló, E., Estelles, V.,  
666 Wang, Y., and Zhu, J.: Spatial distribution of aerosol microphysical and optical properties and direct  
667 radiative effect from the China Aerosol Remote Sensing Network, *Atmos. Chem. Phys.*, 19, 11843-11864,  
668 2019.
- 669 Chen, D.: A monthly circulation climatology for Sweden and its application to a winter temperature case  
670 study, *Int. J. Climatol.*, 20, 1067-1076, 2000.
- 671 Chen, H., and Wang, H.: Haze days in North China and the associated atmospheric circulations based on  
672 daily visibility data from 1960 to 2012, *J. Geophys. Res. Atmos.*, 120, 5895-5909, 2015.
- 673 Chen, S., Zhang, X., Lin, J., Huang, J., Zhao, D., Yuan, T., Huang, K., Luo, Y., Jia, Z., and Zang, Z.:  
674 Fugitive road dust PM<sub>2.5</sub> emissions and their potential health impacts, *Environ. Sci. Technol.*, 53, 8455-  
675 8465, 2019.
- 676 Chen, Z., Chen, D., Zhao, C., Kwan, M.-p., Cai, J., Zhuang, Y., Zhao, B., Wang, X., Chen, B., and Yang,  
677 J.: Influence of meteorological conditions on PM<sub>2.5</sub> concentrations across China: A review of  
678 methodology and mechanism, *Environ. Int.*, 139, 105558, 2020.
- 679 Cheng, Y., He, K.-b., Du, Z.-y., Zheng, M., Duan, F.-k., and Ma, Y.-l.: Humidity plays an important role  
680 in the PM<sub>2.5</sub> pollution in Beijing, *Environ. Pollut.*, 197, 68-75, 2015.
- 681 Notice of the General Office of the State Council on Issuing the Air Pollution Prevention and Control  
682 Action Plan: [http://www.gov.cn/zwggk/2013-09/12/content\\_2486773.htm](http://www.gov.cn/zwggk/2013-09/12/content_2486773.htm), access: 4 August 2020, 2013.
- 683 The State Council rolls out a three-year action plan for clean air: [http://www.gov.cn/zhengce/  
684 content/2018-07/03/content\\_5303158.htm](http://www.gov.cn/zhengce/content/2018-07/03/content_5303158.htm), access: 4 August 2020, 2018.
- 685 Air pollution targeted in 28 cities: [http://www.chinadaily.com.cn/china/2017-  
686 08/26/content\\_31131288.htm](http://www.chinadaily.com.cn/china/2017-08/26/content_31131288.htm), access: 4 August 2020, 2017.
- 687 Ding, A., Huang, X., Nie, W., Chi, X., Xu, Z., Zheng, L., Xu, Z., Xie, Y., Qi, X., and Shen, Y.: Significant  
688 reduction of PM<sub>2.5</sub> in eastern China due to regional-scale emission control: evidence from SORPES in  
689 2011–2018, *Atmos. Chem. Phys.*, 19, 11791-11801, 2019.

690 Fan, L., Yan, Z., Chen, D., and Fu, C.: Comparison between two statistical downscaling methods for  
691 summer daily rainfall in Chongqing, China, *Int. J. Climatol.*, 35, 3781-3797, 2015.

692 Gao, M., Carmichael, G. R., Wang, Y., Saide, P. E., Liu, Z., Xin, J., Shan, Y., and Wang, Z.: Chemical  
693 and Meteorological Feedbacks in the Formation of Intense Haze Events, in: *Air Pollution in Eastern Asia:  
694 An Integrated Perspective*, Springer, 437-452, 2017.

695 Gong, C., and Liao, H.: A typical weather pattern for ozone pollution events in North China, *Atmos.  
696 Chem. Phys.*, 19, 13725-13740, 2019.

697 Gu, Y., Huang, R.-J., Li, Y., Duan, J., Chen, Q., Hu, W., Zheng, Y., Lin, C., Ni, H., and Dai, W.: Chemical  
698 nature and sources of fine particles in urban Beijing: Seasonality and formation mechanisms, *Environ.  
699 Int.*, 140, 105732, 2020.

700 Gui, K., Che, H., Zeng, Z., Wang, Y., Zhai, S., Wang, Z., Luo, M., Zhang, L., Liao, T., and Zhao, H.:  
701 Construction of a virtual PM<sub>2.5</sub> observation network in China based on high-density surface  
702 meteorological observations using the Extreme Gradient Boosting model, *Environ. Int.*, 141, 105801,  
703 2020.

704 Guo, J., Li, Y., Cohen, J. B., Li, J., Chen, D., Xu, H., Liu, L., Yin, J., Hu, K., and Zhai, P.: Shift in the  
705 temporal trend of boundary layer height in China using long-term (1979–2016) radiosonde data,  
706 *Geophys. Res. Lett.*, 46, 6080-6089, 2019.

707 He, J., Zhang, L., Yao, Z., Che, H., Gong, S., Wang, M., Zhao, M., and Jing, B.: Source apportionment  
708 of particulate matter based on numerical simulation during a severe pollution period in Tangshan, North  
709 China, *Environ. Pollut.*, 266, 115133, 2020.

710 Huang, R. J., He, Y., Duan, J., Li, Y., Chen, Q., Zheng, Y., Chen, Y., Hu, W., Lin, C., Ni, H., Dai, W.,  
711 Cao, J., Wu, Y., Zhang, R., Xu, W., Ovadnevaite, J., Ceburnis, D., Hoffmann, T., and O'Dowd, C. D.:  
712 Contrasting sources and processes of particulate species in haze days with low and high relative humidity  
713 in wintertime Beijing, *Atmos. Chem. Phys.*, 20, 9101-9114, 10.5194/acp-20-9101-2020, 2020a.

714 Huang, X., Ding, A., Gao, J., Zheng, B., Zhou, D., Qi, X., Tang, R., Wang, J., Ren, C., and Nie, W.:  
715 Enhanced secondary pollution offset reduction of primary emissions during COVID-19 lockdown in  
716 China, *Natl. Sci. Rev.*, nwaal37, 2020b.

717 Huang, X., Ding, A., Wang, Z., Ding, K., Gao, J., Chai, F., and Fu, C.: Amplified transboundary transport  
718 of haze by aerosol–boundary layer interaction in China, *Nat. Geosci.*, 1-7, 2020c.

719 Huth, R., Beck, C., Philipp, A., Demuzere, M., Ustrnul, Z., Cahynová, M., Kyselý, J., and Tveito, O. E.:  
720 Classifications of atmospheric circulation patterns: recent advances and applications, *Ann. N. Y. Acad.  
721 Sci.*, 1146, 105-152, 2008.

722 Jenkinson, A., and Collison, F.: An initial climatology of gales over the North Sea, *Synoptic climatology  
723 branch memorandum*, 62, 18, 1977.

724 Ji, D., Wang, Y., Wang, L., Chen, L., Hu, B., Tang, G., Xin, J., Song, T., Wen, T., and Sun, Y.: Analysis  
725 of heavy pollution episodes in selected cities of northern China, *Atmos. Environ.*, 50, 338-348, 2012.

726 Jia, Y., Rahn, K. A., He, K., Wen, T., and Wang, Y.: A novel technique for quantifying the regional  
727 component of urban aerosol solely from its sawtooth cycles, *J. Geophys. Res. Atmos.*, 113, D21309, 2008.

728 Jiang, Y., Xin, J., Wang, Y., Tang, G., Zhao, Y., Jia, D., Zhao, D., Wang, M., Dai, L., and Wang, L.: The  
729 dynamic-thermal structures of the planetary boundary layer dominated by synoptic circulations and the  
730 regular effect on air pollution in Beijing, *Atmos. Chem. Phys. Discuss.*, 1-21, 2020.

731 Le, T., Wang, Y., Liu, L., Yang, J., Yung, Y. L., Li, G., and Seinfeld, J. H.: Unexpected air pollution with  
732 marked emission reductions during the COVID-19 outbreak in China, *Science*, 369, 702-706, 2020.

733 Leung, D. M., Mickley, L. J., van Donkelaar, A., Shen, L., and Martin, R. V.: Synoptic meteorological  
734 modes of variability for fine particulate matter (PM<sub>2.5</sub>) air quality in major metropolitan regions of China,  
735 *Atmospheric Chemistry and Physics*, 18, 6733-6748, 2018.

736 Li, H., Zhang, Q., Zhang, Q., Chen, C., Wang, L., Wei, Z., Zhou, S., Parworth, C., Zheng, B., and  
737 Canonaco, F.: Wintertime aerosol chemistry and haze evolution in an extremely polluted city of the North  
738 China Plain: significant contribution from coal and biomass combustion, *Atmos. Chem. Phys.*, 17, 4751-  
739 4768, 2017.

740 Li, J., Li, C., and Zhao, C.: Different trends in extreme and median surface aerosol extinction coefficients  
741 over China inferred from quality-controlled visibility data, *Atmos. Chem. Phys.*, 18, 3289-3298, 2018a.

742 Li, J., Lv, Q., Jian, B., Zhang, M., Zhao, C., Fu, Q., Kawamoto, K., and Zhang, H.: The impact of  
743 atmospheric stability and wind shear on vertical cloud overlap over the Tibetan Plateau, *Atmos. Chem.  
744 Phys.*, 18, 7329-7343, 2018b.

745 Li, J., Liao, H., Hu, J., and Li, N.: Severe particulate pollution days in China during 2013-2018 and the  
746 associated typical weather patterns in Beijing-Tianjin-Hebei and the Yangtze River Delta regions,  
747 *Environ. Pollut.*, 248, 74-81, 2019.

748 Li, M., Wang, L., Liu, J., Gao, W., Song, T., Sun, Y., Li, L., Li, X., Wang, Y., and Liu, L.: Exploring the  
749 regional pollution characteristics and meteorological formation mechanism of PM<sub>2.5</sub> in North China  
750 during 2013-2017, *Environ. Int.*, 134, 105283, 2020.

751 Li, Q., Zhang, R., and Wang, Y.: Interannual variation of the wintertime fog-haze days across central and  
752 eastern China and its relation with East Asian winter monsoon, *Int. J. Climatol.*, 36, 346-354, 2016.

753 Li, W., Shao, L., and Buseck, P.: Haze types in Beijing and the influence of agricultural biomass burning,  
754 *Atmos. Chem. Phys.*, 10, 2010.

755 Liu, C., Zhang, F., Miao, L., Lei, Y., and Yang, Q.: Future haze events in Beijing, China: When climate  
756 warms by 1.5 and 2.0° C, *Int. J. Climatol.*, 40, 3689-3700, 2019.

757 Ma, J., and Zhang, R.: Opposite interdecadal variations of wintertime haze occurrence over North China  
758 Plain and Yangtze River Delta regions in 1980-2013, *Sci. Total Environ.*, 139240, 2020.

759 Ma, Y., Ye, J., Xin, J., Zhang, W., Vilà-Guerau de Arellano, J., Wang, S., Zhao, D., Dai, L., Ma, Y., and  
760 Wu, X.: The stove, dome, and umbrella effects of atmospheric aerosol on the development of the  
761 planetary boundary layer in hazy regions, *Geophys. Res. Lett.*, 47, e2020GL087373, 2020.

762 Miao, Y., Che, H., Zhang, X., and Liu, S.: Integrated impacts of synoptic forcing and aerosol radiative  
763 effect on boundary layer and pollution in the Beijing-Tianjin-Hebei region, China, *Atmos. Chem. Phys.*,  
764 20, 5899-5909, 2020.

- 765 Mu, M., and Zhang, R.: Addressing the issue of fog and haze: A promising perspective from  
766 meteorological science and technology, *Sci. China Earth Sci.*, 57, 1-2, 2014.
- 767 Pei, L., and Yan, Z.: Diminishing clear winter skies in Beijing towards a possible future, *Environ. Res.*  
768 *Lett.*, 13, 124029, 2018.
- 769 Pei, L., Yan, Z., Sun, Z., Miao, S., and Yao, Y.: Increasing persistent haze in Beijing: potential impacts  
770 of weakening East Asian winter monsoons associated with northwestern Pacific sea surface temperature  
771 trends, *Atmos. Chem. Phys.*, 18, 3173–3183, 2018.
- 772 Pei, L., Yan, Z., Chen, D., and Miao, S.: Climate variability or anthropogenic emissions: which caused  
773 Beijing Haze?, *Environ. Res. Lett.*, 15, 034004, 2020.
- 774 Philipp, A., Beck, C., Esteban, P., Kreienkamp, F., Krennert, T., Lochbihler, K., Lykoudis, S. P., Pianko-  
775 Kluczynska, K., Post, P., and Alvarez10, D. R.: cost733class-1.2 User guide, Augsburg, Germany, 10-21,  
776 2014.
- 777 Quan, J., Dou, Y., Zhao, X., Liu, Q., Sun, Z., Pan, Y., Jia, X., Cheng, Z., Ma, P., and Su, J.: Regional  
778 atmospheric pollutant transport mechanisms over the North China Plain driven by topography and  
779 planetary boundary layer processes, *Atmos. Environ.*, 221, 117098, 2020.
- 780 Shi, X., and Brasseur, G. P.: The Response in Air Quality to the Reduction of Chinese Economic  
781 Activities during the COVID-19 Outbreak, *Geophys. Res. Lett.*, e2020GL088070, 2020.
- 782 Sun, Y., Jiang, Q., Wang, Z., Fu, P., Li, J., Yang, T., and Yin, Y.: Investigation of the sources and evolution  
783 processes of severe haze pollution in Beijing in January 2013, *J. Geophys. Res. Atmos.*, 119, 4380-4398,  
784 2014.
- 785 Tang, G., Zhang, J., Zhu, X., Song, T., Munkel, C., Hu, B., Schäfer, K., Liu, Z., Zhang, J., and Wang, L.:  
786 Mixing layer height and its implications for air pollution over Beijing, China, *Atmos. Chem. Phys.*, 16,  
787 2459, 2016a.
- 788 Tang, L., Yu, H., Ding, A., Zhang, Y., Qin, W., Wang, Z., Chen, W., Hua, Y., and Yang, X.: Regional  
789 contribution to PM1 pollution during winter haze in Yangtze River Delta, China, *Sci. Total Environ.*, 541,  
790 161-166, 2016b.
- 791 Tie, X., Zhang, Q., He, H., Cao, J., Han, S., Gao, Y., Li, X., and Jia, X. C.: A budget analysis of the  
792 formation of haze in Beijing, *Atmos. Environ.*, 100, 25-36, 2015.
- 793 Valverde, V., Pay, M. T., and Baldasano, J. M.: Circulation-type classification derived on a climatic basis  
794 to study air quality dynamics over the Iberian Peninsula, *Int. J. Climatol.*, 35, 2877-2897, 2015.
- 795 Wang, H., Chen, H., and Liu, J.: Arctic sea ice decline intensified haze pollution in eastern China, *Atmos.*  
796 *Oceanic Sci. Lett.*, 8, 1-9, 2015.
- 797 Wang, J., Liu, Y., and Ding, Y.: On the connection between interannual variations of winter haze  
798 frequency over Beijing and different ENSO flavors, *Sci. Total Environ.*, 140109, 2020a.
- 799 Wang, P., Chen, K., Zhu, S., Wang, P., and Zhang, H.: Severe air pollution events not avoided by reduced  
800 anthropogenic activities during COVID-19 outbreak, *Resour. Conserv. Recycl.*, 158, 104814, 2020b.
- 801 Wang, T., Nie, W., Gao, J., Xue, L., Gao, X., Wang, X., Qiu, J., Poon, C., Meinardi, S., and Blake, D.:

802 Air quality during the 2008 Beijing Olympics: secondary pollutants and regional impact, *Atmos. Chem.*  
803 *Phys.*, 10, 7603-7615, 2010.

804 Wang, X., Wang, K., and Su, L.: Contribution of atmospheric diffusion conditions to the recent  
805 improvement in air quality in China, *Sci. Rep.*, 6, 36404, 2016.

806 Wang, X., Dickinson, R. E., Su, L., Zhou, C., and Wang, K.: PM2.5 pollution in China and how it has  
807 been exacerbated by terrain and meteorological conditions, *Bull. Am. Meteorol. Soc.*, 99, 105-119, 2018.

808 Wang, X., Wei, H., Liu, J., Xu, B., Wang, M., Ji, M., and Jin, H.: Quantifying the light absorption and  
809 source attribution of insoluble light-absorbing particles on Tibetan Plateau glaciers between 2013 and  
810 2015, *Cryosphere*, 13, 309-324, 2019a.

811 Wang, X., Zhang, R., and Yu, W.: The effects of PM2.5 concentrations and relative humidity on  
812 atmospheric visibility in Beijing, *J. Geophys. Res. Atmos.*, 124, 2235-2259, 2019b.

813 Wang, X., and Zhang, R.: Effects of atmospheric circulations on the interannual variation in PM2.5  
814 concentrations over the Beijing-Tianjin-Hebei region in 2013-2018, *Atmos. Chem. Phys.*, 20, 7667-  
815 7682, 2020a.

816 Wang, X., and Zhang, R.: How Does Air Pollution Change during COVID-19 Outbreak in China?, *Bull.*  
817 *Am. Meteorol. Soc.*, 1-12, 2020b.

818 Wang, Y., Duan, J., Xie, X., He, Q., Cheng, T., Mu, H., Gao, W., and Li, X.: Climatic factors and their  
819 availability in estimating long-term variations of fine particle distributions over East China, *J.*  
820 *Geophys. Res. Atmos.*, 124, 3319-3334, 2019c.

821 Wang, Y., Li, W., Gao, W., Liu, Z., Tian, S., Shen, R., Ji, D., Wang, S., Wang, L., and Tang, G.: Trends  
822 in particulate matter and its chemical compositions in China from 2013-2017, *Sci. China Earth Sci.*, 62,  
823 1857-1871, 2019d.

824 Wang, Y., Yu, M., Wang, Y., Tang, G., Song, T., Zhou, P., Liu, Z., Hu, B., Ji, D., and Wang, L.: Rapid  
825 formation of intense haze episodes via aerosol-boundary layer feedback in Beijing, *Atmos. Chem. Phys.*,  
826 20, 45-53, 2020c.

827 Wu, P., Ding, Y., and Liu, Y.: Atmospheric circulation and dynamic mechanism for persistent haze events  
828 in the Beijing-Tianjin-Hebei region, *Adv. Atmos. Sci.*, 34, 429-440, 2017.

829 Xia, X., Che, H., Zhu, J., Chen, H., Cong, Z., Deng, X., Fan, X., Fu, Y., Goloub, P., and Jiang, H.:  
830 Ground-based remote sensing of aerosol climatology in China: Aerosol optical properties, direct  
831 radiative effect and its parameterization, *Atmos. Environ.*, 124, 243-251, 2016.

832 Xin, J., Wang, Y., Wang, L., Tang, G., Sun, Y., Pan, Y., and Ji, D.: Reductions of PM2.5 in Beijing-  
833 Tianjin-Hebei urban agglomerations during the 2008 Olympic Games, *Adv. Atmos. Sci.*, 29, 1330-1342,  
834 2012.

835 Xin, J., Gong, C., Wang, S., and Wang, Y.: Aerosol direct radiative forcing in desert and semi-desert  
836 regions of northwestern China, *Atmos. Res.*, 171, 56-65, 2016.

837 Xu, J., Chang, L., Qu, Y., Yan, F., Wang, F., and Fu, Q.: The meteorological modulation on PM2.5  
838 interannual oscillation during 2013 to 2015 in Shanghai, China, *Sci. Total Environ.*, 572, 1138-1149,

839 2016.

840 Yao, L., Garmash, O., Bianchi, F., Zheng, J., Yan, C., Kontkanen, J., Junninen, H., Mazon, S. B., Ehn,  
841 M., and Paasonen, P.: Atmospheric new particle formation from sulfuric acid and amines in a Chinese  
842 megacity, *Science*, 361, 278-281, 2018.

843 Zhang, F., Wang, Y., Peng, J., Chen, L., Sun, Y., Duan, L., Ge, X., Li, Y., Zhao, J., and Liu, C.: An  
844 unexpected catalyst dominates formation and radiative forcing of regional haze, *Proc. Natl. Acad. Sci.*  
845 *USA*, 117, 3960-3966, 2020.

846 Zhang, K., Ma, Y., Xin, J., Liu, Z., Ma, Y., Gao, D., Wu, J., Zhang, W., Wang, Y., and Shen, P.: The  
847 aerosol optical properties and PM<sub>2.5</sub> components over the world's largest industrial zone in Tangshan,  
848 North China, *Atmos. Res.*, 201, 226-234, 2018a.

849 Zhang, Q., Zheng, Y., Tong, D., Shao, M., Wang, S., Zhang, Y., Xu, X., Wang, J., He, H., and Liu, W.:  
850 Drivers of improved PM<sub>2.5</sub> air quality in China from 2013 to 2017, *Proc. Natl. Acad. Sci. USA*, 116,  
851 24463-24469, 2019a.

852 Zhang, R., Sumi, A., and Kimoto, M.: Impact of El Niño on the east Asian monsoon: A diagnostic study  
853 of the '86-87 and '91-92 events, *J. Meteorol. Soc. Japan*, 74, 49-62, 1996.

854 Zhang, R., Li, Q., and Zhang, R.: Meteorological conditions for the persistent severe fog and haze event  
855 over eastern China in January 2013, *Sci. China Earth Sci.*, 57, 26-35, 2014.

856 Zhang, R.: Warming boosts air pollution, *Nat. Clim. Change*, 7, 238-239, 2017.

857 Zhang, X., Zhong, J., Wang, J., Wang, Y., and Liu, Y.: The interdecadal worsening of weather conditions  
858 affecting aerosol pollution in the Beijing area in relation to climate warming, *Atmos. Chem. Phys.*, 18,  
859 5991-5999, 2018b.

860 Zhang, X., Xu, X., Ding, Y., Liu, Y., Zhang, H., Wang, Y., and Zhong, J.: The impact of meteorological  
861 changes from 2013 to 2017 on PM<sub>2.5</sub> mass reduction in key regions in China, *Sci. China Earth Sci.*, 62,  
862 1885-1902, 2019b.

863 Zhang, Z., Gong, D., Mao, R., Kim, S.-J., Xu, J., Zhao, X., and Ma, Z.: Cause and predictability for the  
864 severe haze pollution in downtown Beijing in November–December 2015, *Sci. Total Environ.*, 592, 627-  
865 638, 2017.

866 Zhao, C., Li, Y., Zhang, F., Sun, Y., and Wang, P.: Growth rates of fine aerosol particles at a site near  
867 Beijing in June 2013, *Adv. Atmos. Sci.*, 35, 209-217, 2018a.

868 Zhao, C., Wang, Y., Shi, X., Zhang, D., Wang, C., Jiang, J. H., Zhang, Q., and Fan, H.: Estimating the  
869 contribution of local primary emissions to particulate pollution using high-density station observations,  
870 *J. Geophys. Res. Atmos.*, 124, 1648-1661, 2019.

871 Zhao, C., Yang, Y., Fan, H., Huang, J., Fu, Y., Zhang, X., Kang, S., Cong, Z., Letu, H., and Menenti, M.:  
872 Aerosol characteristics and impacts on weather and climate over the Tibetan Plateau, *Natl. Sci. Rev.*, 7,  
873 492-495, 2020a.

874 Zhao, D., Schmitt, S. H., Wang, M., Acir, I.-H., Tillmann, R., Tan, Z., Novelli, A., Fuchs, H., Pullinen,  
875 I., and Wegener, R.: Effects of NO<sub>x</sub> and SO<sub>2</sub> on the secondary organic aerosol formation from

876 photooxidation of alpha-pinene and limonene, *Atmos. Chem. Phys.*, 18, 1611–1628, 2018b.

877 Zhao, G., Zhao, C., Kuang, Y., Tao, J., Tan, W., Bian, Y., Li, J., and Li, C.: Impact of aerosol hygroscopic  
878 growth on retrieving aerosol extinction coefficient profiles from elastic-backscatter lidar signals, *Atmos.*  
879 *Chem. Phys.*, 17, 12133-12143, 2017.

880 Zhao, H., Che, H., Zhang, L., Gui, K., Ma, Y., Wang, Y., Wang, H., Zheng, Y., and Zhang, X.: How  
881 aerosol transport from the North China plain contributes to air quality in northeast China, *Sci. Total*  
882 *Environ.*, 139555, 2020b.

883 Zheng, B., Tong, D., Li, M., Liu, F., Hong, C., Geng, G., Li, H., Li, X., Peng, L., and Qi, J.: Trends in  
884 China's anthropogenic emissions since 2010 as the consequence of clean air actions, *Atmos. Chem. Phys.*,  
885 18, 14095-14111, 2018.

886 Zheng, G., Duan, F., Su, H., Ma, Y., Cheng, Y., Zheng, B., Zhang, Q., Huang, T., Kimoto, T., and Chang,  
887 D.: Exploring the severe winter haze in Beijing: the impact of synoptic weather, regional transport and  
888 heterogeneous reactions, *Atmos. Chem. Phys.*, 15, 2969, 2015.

889 Zhu, X., Tang, G., Hu, B., Wang, L., Xin, J., Zhang, J., Liu, Z., Munkel, C., and Wang, Y.: Regional  
890 pollution and its formation mechanism over North China Plain: A case study with ceilometer  
891 observations and model simulations, *J. Geophys. Res. Atmos.*, 121, 14,574-514,588, 2016.

892

893 Table 1. Frequency of the relative day-to-day PM2.5 difference within the specific range.

Relative Difference (%)	<-80	-80~-60	-60~-40	-40~-20	-20~0	0~40	40~80	80~120	>120
MAM	0.4	4.4	9.0	13.5	17.2	31.6	14.3	5.4	3.8
JJA	0.2	2.2	7.6	15.6	20.7	34.9	12.0	4.3	2.3
SON	1.3	5.2	9.1	12.2	14.8	29.4	15.2	6.7	5.7
DJF	1.9	6.7	9.7	12.5	13.1	25.2	15.3	7.9	7.2

894

895

896 Table 2. The average relative difference of PM2.5 concentrations before and after the occurrence of  
 897 decay processes (i.e.,  $(PM_t - PM_{t-1}) / PM_{t-1} * 100$ , where  $PM_t$  is the daily mean PM2.5 concentration on  
 898 the decay phase day).

%	CT1	CT2	CT3	Wet deposition
MAM	-37.2	-44.8	-28.2	-40
JJA	-34.5	-20.4	//	-26.2
SON	-40.1	-42.9	-26.9	-35.8
DJF	-36.9	-41	-29.3	-43.9

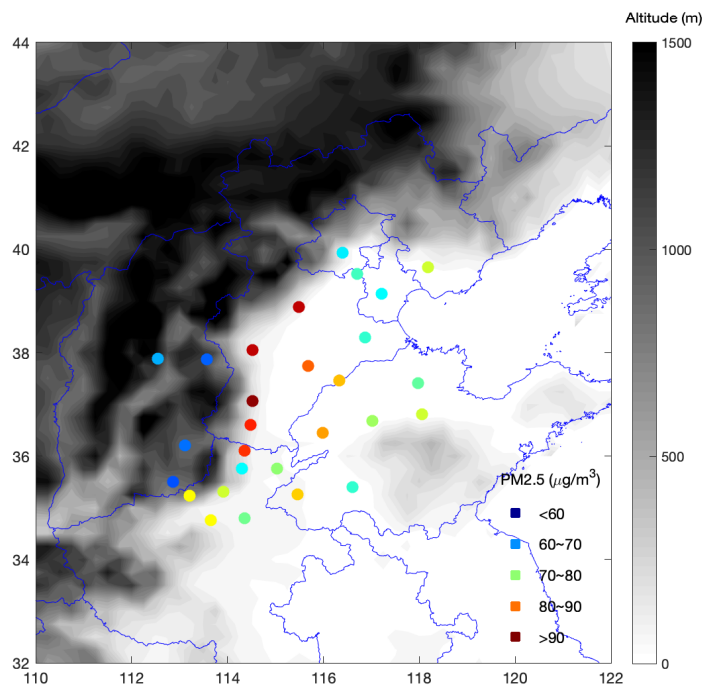
899

900

带格式的: 左对齐, 缩进: 首行缩进: 0 字符, 空格  
 段前: 0 磅, 行距: 单线, 孤行控制



901



902

903 Figure 1. Distribution of annual mean PM2.5 concentrations in the 28 cities by altitude. The PM2.5  
 904 concentration is the annual mean value from 2014 to 2019 (units:  $\mu\text{g}/\text{m}^3$ ). The elevation over the  
 905 domain was obtained from Global Digital Elevation Model with a resolution of  $0.5^\circ \times 0.5^\circ$ .

906

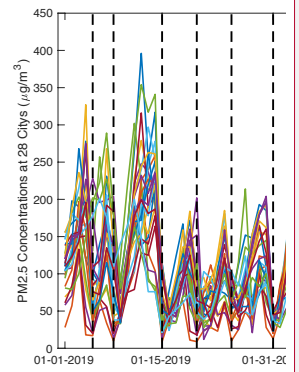
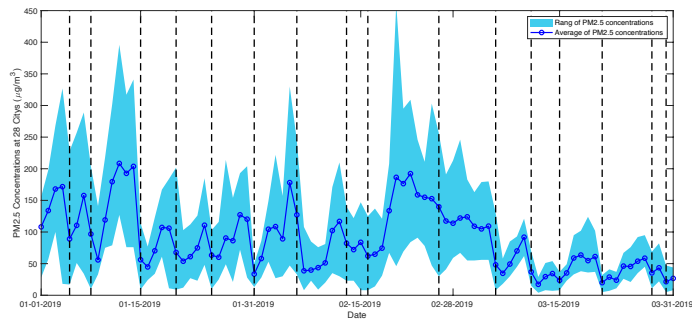
删除的内容: .

带格式的: 缩进: 首行缩进: 0 字符

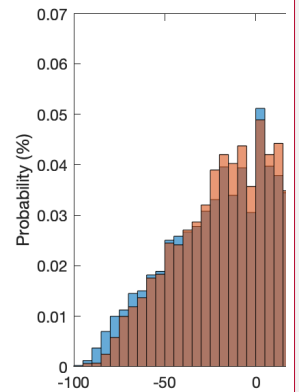
删除的内容: Annual mean

删除的内容: s

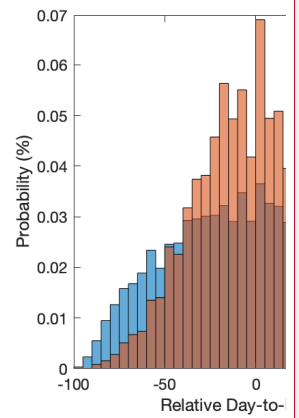
删除的内容: in the 28 pollution channel cities of Beijing



删除的内容:



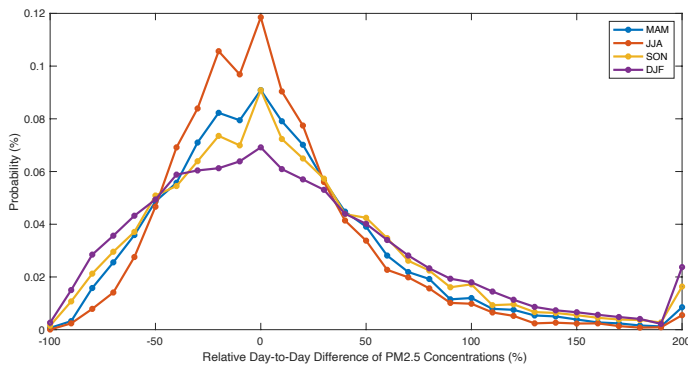
删除的内容:



912

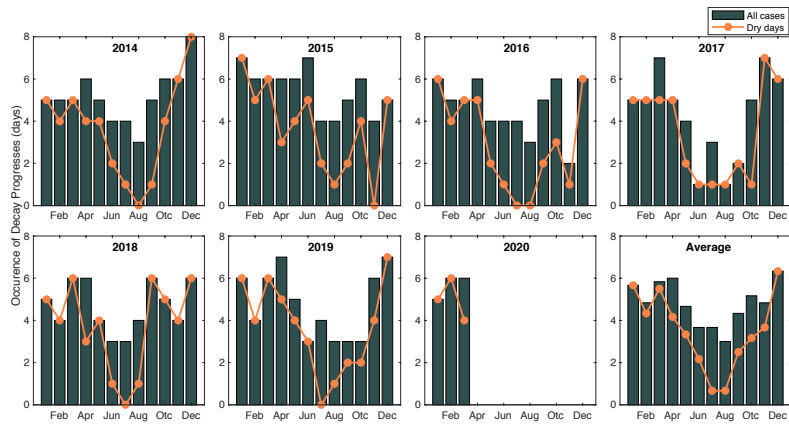
913 Figure 2. Time series of daily mean PM2.5 concentrations in the 28 pollution channel cities from  
914 January to March 2019 (units:  $\mu\text{g}/\text{m}^3$ ).

915



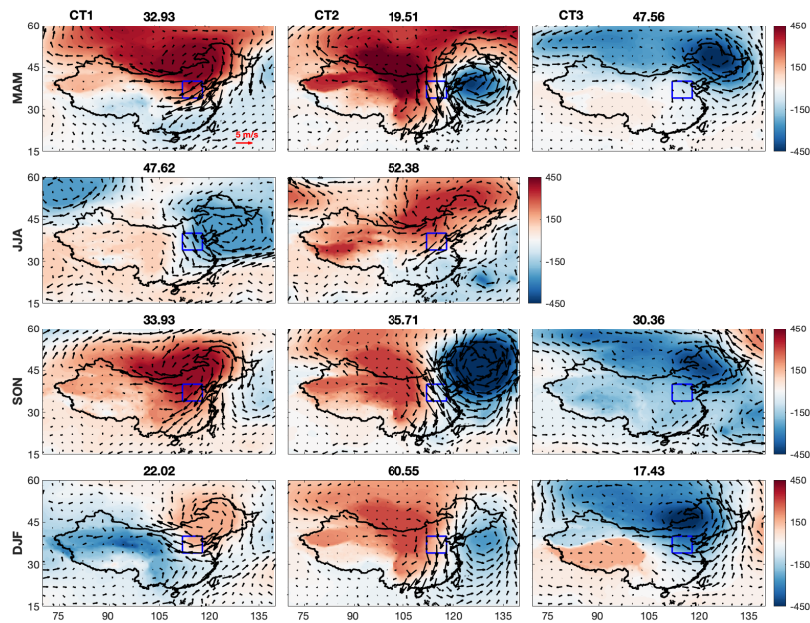
916

917 Figure 3. Probability distribution of the relative day-to-day difference of PM2.5 concentrations. The  
918 relative difference is based on the PM2.5 concentration on the previous day. The distributions in  
919 spring and autumn are combined in the upper panel, and cases in winter and summer are shown at  
920 the bottom.



923

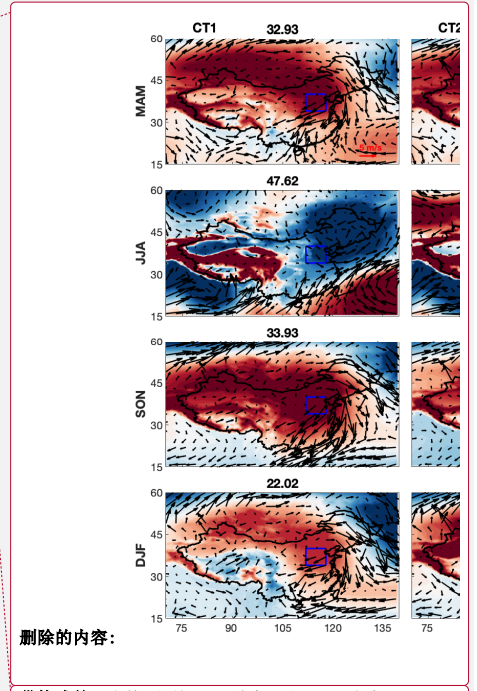
924 Figure 4. Monthly cumulative occurrence of the decay processes of pollution episodes. The orange  
 925 curve indicates the decay process occurrences on dry days. In total, 365 decay processes are  
 926 identified from January 2014 to March 2020, and 97 of them are associated with precipitation levels  
 927 greater than 10 mm/day.  
 928



930

931 Figure 5. Distribution of the geopotential height anomalies (shaded, unit:  $m^2/s^2$ ) and wind field  
 932 anomalies at 925 hPa for each circulation type. The number over each subplot indicates the  
 933 occurrence frequency of the specific circulation type. The solid blue box is the location of the  
 934 domain region covering the 28 pollution channel cities.

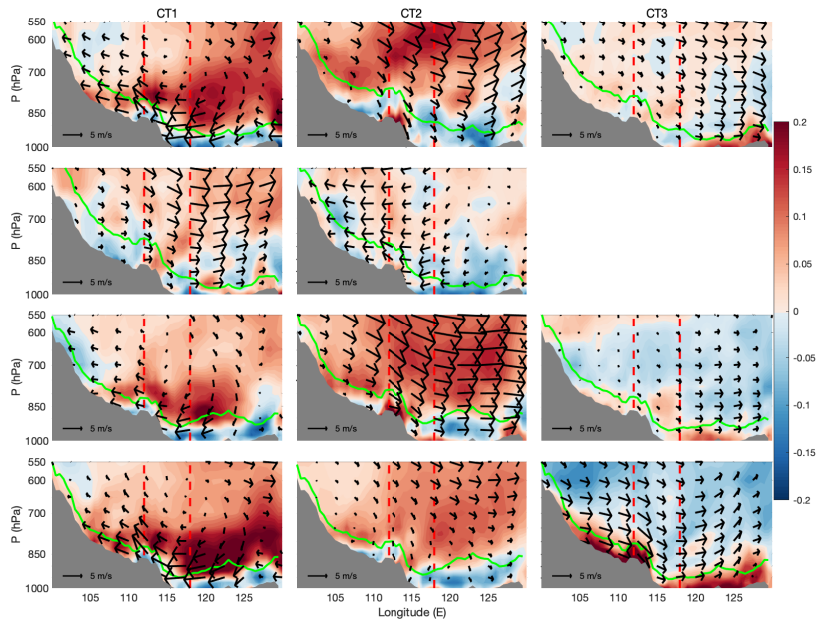
935



删除的内容:

带格式的: 空格 段前: 1 线条, 行距: 多个 1.15 li

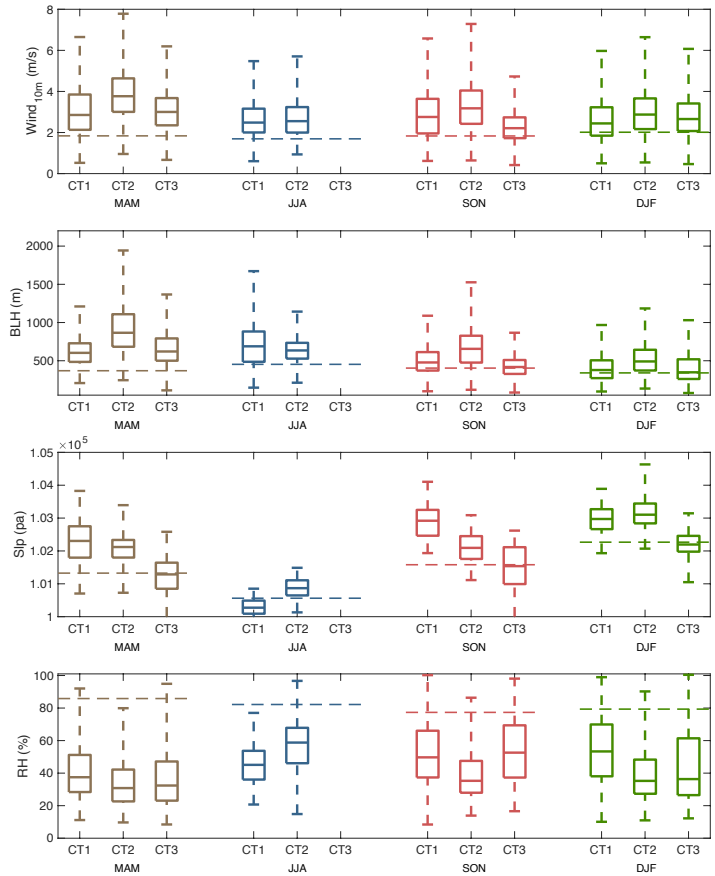
删除的内容: 6



939

940 Figure 6. Zonal averaged profile of the distribution of vertical wind shear anomalies in the domain  
 941 region (shaded, units:  $\text{m}/(\text{s}\cdot 100 \text{ m})$ ) and the vertical and zonal circulation anomalies. The green line  
 942 indicates the average location of the top of the boundary layer. Zonal wind shear, circulation and  
 943 boundary layer height are the average values between  $34\text{-}40^\circ \text{ N}$ . The two dashed lines are the eastern  
 944 and western boundaries of the domain ( $112$  to  $118^\circ \text{ E}$ ). The grey region indicates the average altitude  
 945 between  $34\text{-}40^\circ \text{ N}$ .

删除的内容: 7



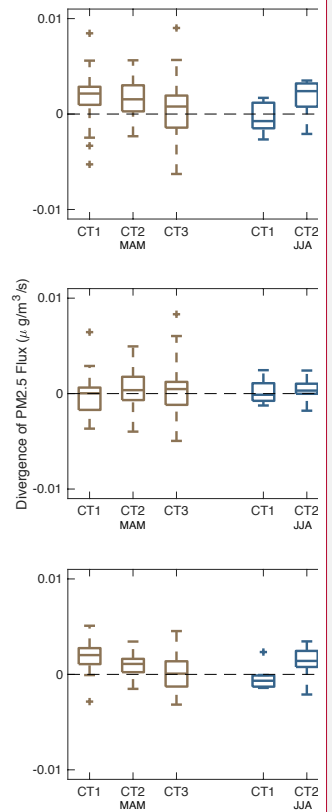
947

948 Figure 7. Boxplot of surface wind speed, boundary layer height (BLH), sea level pressure (slp) and  
 949 relative humidity (RH) for each circulation type. The dashed line indicates the seasonal mean of the  
 950 specific variables. The mean values of all of the meteorological variables in each CT are  
 951 significantly different with their seasonal mean based on two-tail student-t test at a significant level  
 952 of 0.01.

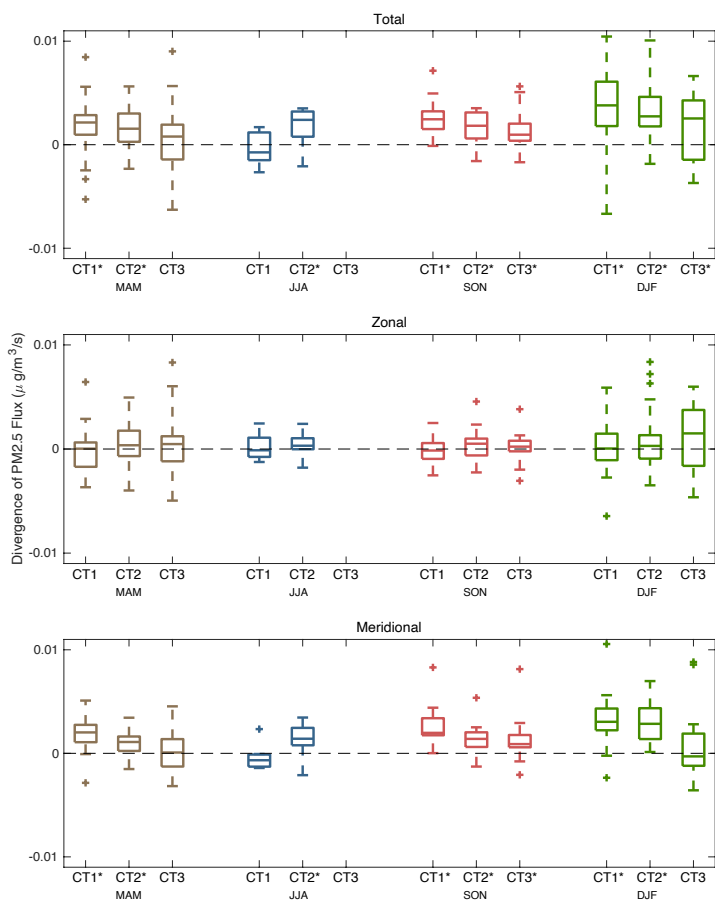
953

删除的内容: 8

删除的内容:



删除的内容:

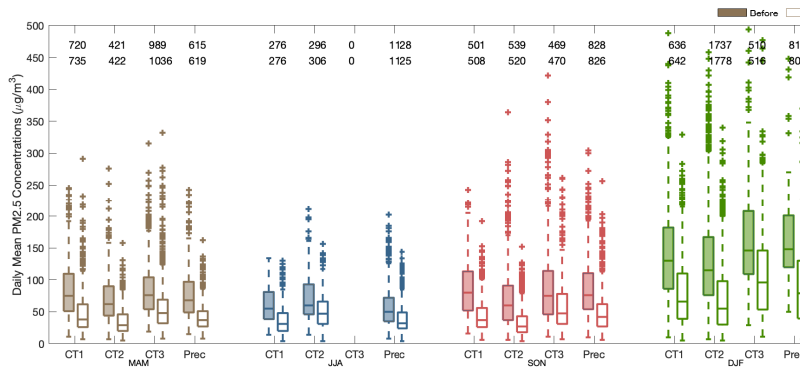


957

958 Figure 8. Boxplot of the divergence of PM2.5 flux over the region of 34-40° N and 112-118° E. The  
 959 daily divergence is calculated based on the Eq. (1). Zonal and meridional components are the first  
 960 and second terms of the formula. \* in the x axis marks the divergence in a specific CT is significantly  
 961 different with zero based on two-tail student-t test at a significant level of 0.01.

删除的内容: 9

删除的内容:

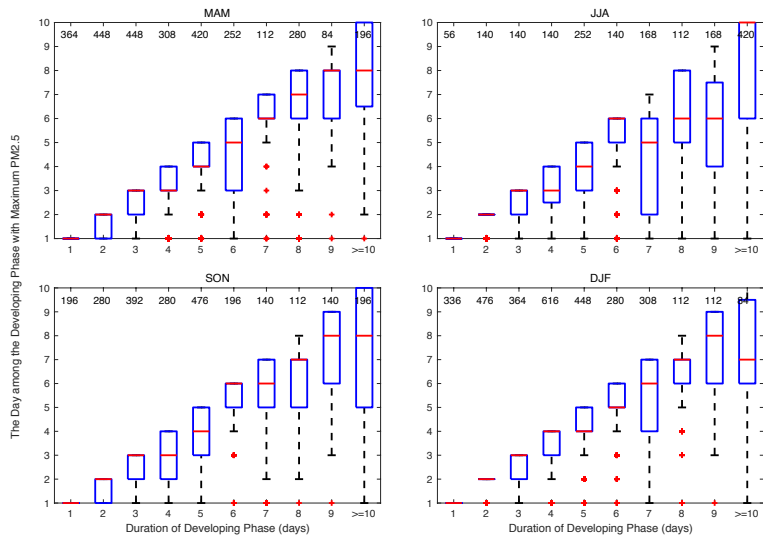


964

965 Figure 9. Distribution of the daily mean PM<sub>2.5</sub> concentrations before and after the occurrence of  
 966 decay processes of pollution episodes in the 28 pollution channel cities. The hollow box indicates  
 967 the concentration on the decay phase day, and the solid box is the value on the previous day. The  
 968 relative differences in the PM<sub>2.5</sub> concentrations after the occurrence of decay process are  
 969 summarized in Table 2. The number at the top of each box indicates the sample size used for the  
 970 boxplot. The number in the first line is the sample size of the “before” case; and the second line is  
 971 for the “after” case.  
 972

删除的内容: 10

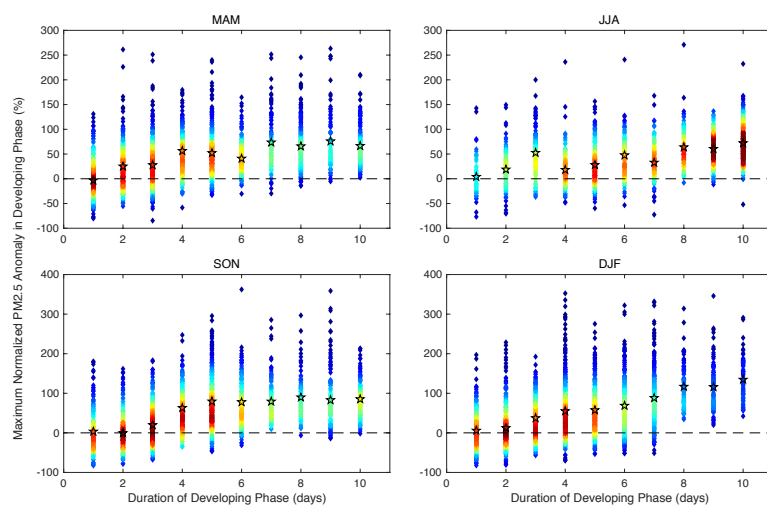




974

975 Figure 10. The day of the maximum PM2.5 concentration during each pollution episode varies with  
 976 the duration of the developing phase.  
 977

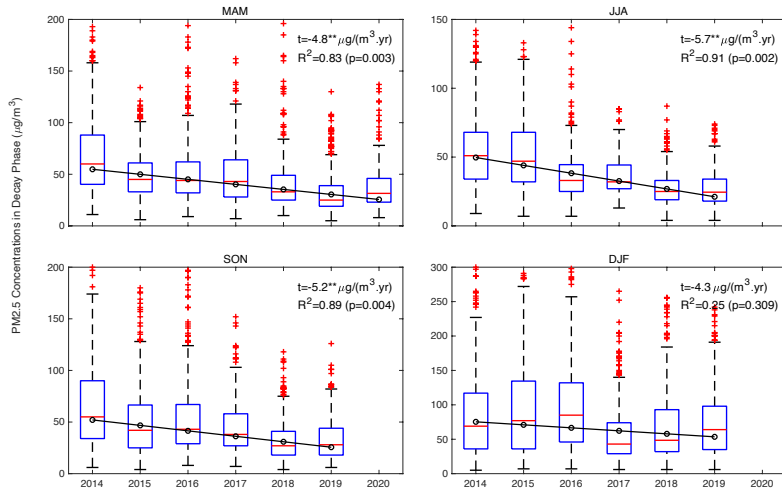
删除的内容: 1



979

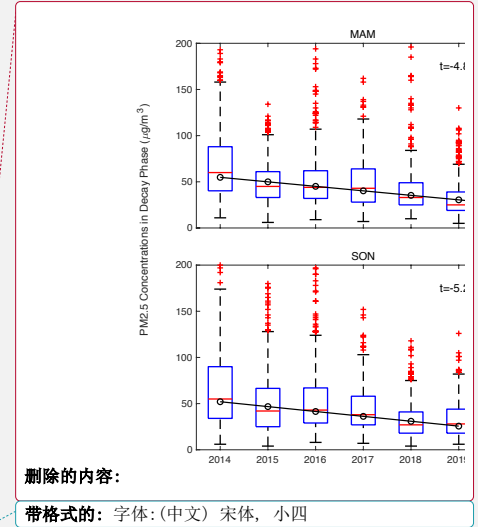
980 Figure 11. The density plot of the maximum PM2.5 concentration according to the duration of the  
 981 developing phase of pollution episodes. Daily PM2.5 concentrations are normalized by their  
 982 monthly mean value to exclude the effects of seasonal and interannual variations in air quality. A  
 983 warmer color indicates a higher density of scatter. Pentagrams mark the average maximum PM2.5  
 984 concentration for the specific duration period.  
 985

删除的内容: 2



988

989 Figure 12. Variations in the average PM2.5 concentration on all the decay phase days from 2014 to  
 990 2020. The black hollow circles indicate the mean PM2.5 concentration in each year. The black line  
 991 is the fitting line based on the monthly median value. The number in the subplot is the linear trend  
 992 (t), R-square and p-value of least squares regression model. \*\* after linear trend indicates the linear  
 993 regression model is significant with a p-value<0.01.



删除的内容:

带格式的: 字体:(中文) 宋体, 小四

删除的内容: 3

删除的内容: Variations in the average PM2.5 concentration on all the decay phase days from 2014 to 2020. The black hollow circles indicate the mean PM2.5 concentration in each year. The black line is the fitting line based on the mean value. The number in the subplot is the linear trend of the fitting line.